

SAMPLE-EFFICIENT LEARNING OF CONCEPTS WITH THEORETICAL GUARANTEES: FROM DATA TO CONCEPTS WITHOUT INTERVENTIONS

Hidde Fokkema

Tim van Erven*

Korteweg-de Vries Institute for Mathematics, University of Amsterdam

H.J.FOKKEMA@UVA.NL

TIM@TIMVANERVEN.NL

Sara Magliacane*

Informatics Institute, University of Amsterdam

S.MAGLIACANE@UVA.NL

Abstract

Machine learning is a vital part of many real-world systems, but several concerns remain about the lack of interpretability, explainability and robustness of black-box AI systems. Concept-based models (CBM) address some of these challenges by learning interpretable *concepts* from high-dimensional data, e.g. images, which are used to predict labels. An important issue in CBMs is *concept leakage*, i.e., spurious information in the learned concepts, which effectively leads to learning “wrong” concepts. Current mitigating strategies are heuristic, have strong assumptions, e.g., they assume that the concepts are statistically independent of each other, or require substantial human interaction in terms of both interventions and labels provided by annotators. In this paper, we describe a framework that provides theoretical guarantees on the correctness of the learned concepts and on the number of required labels, without requiring any interventions. Our framework leverages causal representation learning (CRL) to learn high-level causal variables from low-level data, and learns to align these variables with interpretable concepts. We propose a linear and a non-parametric estimator for this mapping, providing a finite-sample high probability result in the linear case and an asymptotic consistency result for the non-parametric estimator. We implement our framework with state-of-the-art CRL methods, and show its efficacy in learning the correct concepts in synthetic and image benchmarks.

Keywords: Interpretability; Concepts; Causal Representation Learning.

1 Introduction

Machine learning is a vital part of many real-world systems, but concerns remain about the lack of interpretability, robustness and adherence to regulations of current systems (Bengio et al., 2025). These issues might be exacerbated by the lack of guarantees in explaining the behavior of AI systems in terms of human interpretable, high-level *concepts*.

The field of interpretable machine learning and explainable AI have developed many techniques to interpret models and explain their predictions (Molnar, 2022), either by extracting known concepts from the internals of black-box models (Kim et al., 2018; Goyal et al., 2019; Graziani et al., 2023; Lovering and Pavlick, 2022), or by building the explicit use of concepts into the internals of these systems, e.g. as in *concept-based models* (CBM) (Koh et al., 2020; Ismail et al., 2023; Marconato et al., 2022; Zarlenga et al., 2022).

An advantage of CBMs is that they can provide similar accuracy in terms of prediction, while also ensuring interpretability by construction, as opposed to post-hoc methods (Belinkov, 2022). On the other hand, CBMs are susceptible to *concept leakage* Margeloiu et al. (2021); Mahinpei et al. (2021), i.e. a learned concept can potentially encode information that is unrelated to its intended meaning, even with concept-level supervision. This is particularly problematic if there exist spurious correlations between concepts in the training dataset. The CBM model might rely on this correlation when learning two concepts (e.g. learning to associate the “Cow” concept with mountains, if we train on a dataset of images from Switzerland), which would then fail in a different setting where this correlation does not appear.

*Equal contribution

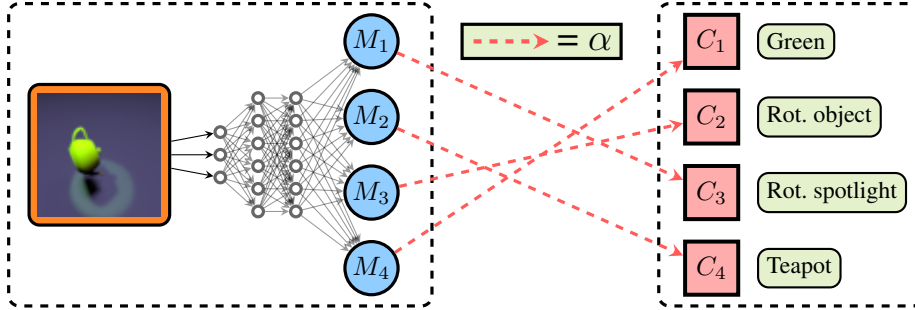


Figure 1: An overview of our framework: we aim to provide theoretical guarantees for concepts learned from data in terms of correctness and required numbers of labelled data by leveraging the disentangled representations M_j provided by causal representation learning methods (left box) and learning an alignment map α to the concepts C_i (right box).

Most current mitigating strategies for concept leakage are heuristic [Alvarez-Melis and Jaakkola \(2018\)](#); [Chen et al. \(2020\)](#). An exception are [Marconato et al. \(2022\)](#), who leverage disentangled representation learning to ensure leak-proof CBMs, but assume independent concepts. [Marconato et al. \(2023\)](#) allow for some type of dependence between concepts, but they require interventions on the data generating process, for which they require annotations. None of these works provide guarantees in terms of correctness of the learned concepts or the number of labels.

In this paper, we describe a general framework that provides theoretical guarantees on the correctness of the learned concepts and on the number of required labels, without requiring any interventions. Our framework leverages state-of-the-art CRL methods ([Khemakhem et al., 2020](#); [Lachapelle et al., 2022](#); [Lippe et al., 2022](#)), to learn high-level causal variables from low-level unlabelled data, e.g. images, with identifiability guarantees. We assume that the ground truth high-level causal variables correspond to the concepts that we would like to learn. Typically, CRL methods only provide *identifiability up to permutation and element-wise transformations*, so we need to learn an alignment map from the learned embeddings M_i to the concepts C_j , which consists of a permutation and a set of simple functions, as shown in Figure 1. We leverage techniques from high-dimensional statistics ([Bühlmann and Van De Geer, 2011](#); [Bach, 2008](#)) to provide theoretical guarantees for this alignment map.

In particular, we propose both a linear and a non-parametric estimator for this mapping based on a convex optimization problem with a Group Lasso regularization ([Yuan and Lin, 2006](#)). The first method is based on group regularized linear regression, with the possibility to incorporate a feature map, and comes with a high probability result on its correctness. This result comes with an explicit dependence on all the relevant parameters. In particular, the dependence on the number of data points allows a practitioner to tune the regularization parameter in a principled way. This allows for good results even with a small number of data points. The second method is based on a kernelized procedure, allowing for more flexibility, but comes with asymptotic guarantees instead of finite sample guarantees. We implement our framework with state-of-the-art CRL methods, and show its efficacy in learning the correct concepts in synthetic and image benchmarks from the CRL literature with few labels.

2 Related Work

Extracting high-level concepts from the inner workings of machine learning models has gained traction over the last years ([Alain and Bengio, 2017](#); [Ghorbani et al., 2019](#); [McGrath et al., 2022](#)). These concepts can be used to create interpretable explanations. In Concept Based Models (CBMs), the concepts are hard coded in the structure of the model ([Koh et al., 2020](#); [Marconato et al., 2022](#); [Ismail et al., 2023](#); [Zarlenga et al., 2022](#)). The explanations can be constructed by looking at the activations for a prediction of the components where the concepts are hard coded. The benefit of this approach is that the concept is faithfully represented in the model

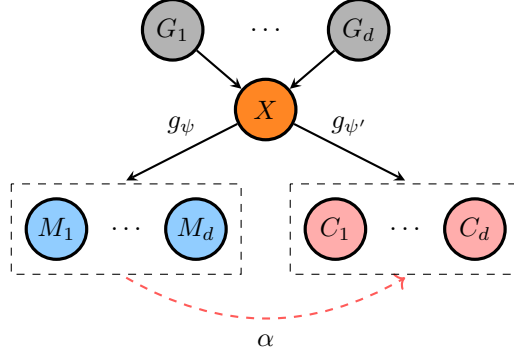


Figure 2: Data generating process, where G_i are the ground truth causal variables, X is an observation, M_i represent the representations learned through the encoder g_ψ , C_j represent the concepts and α is the alignment map.

and explanation. One of the caveats is that in the case of concept leakage [Margeloiu et al. \(2021\)](#); [Mahinpei et al. \(2021\)](#), which can happen even with concept-level supervision, the concepts might be learned incorrectly.

Most current mitigating strategies for concept leakage are heuristic, e.g. encouraging sparsity [Alvarez-Melis and Jaakkola \(2018\)](#) or orthonormality of the concepts [Chen et al. \(2020\)](#). Our work takes inspiration from [Marconato et al. \(2022\)](#) who leverage disentangled representation learning to learn an embedding of ground truth concepts that can be then aligned with the concept labels to ensure no concept leakage in CBMs. This work assumes that the concepts are independent in the dataset, but [Marconato et al. \(2023\)](#) consider a simplified version of causal representation learning (CRL) methods [Schölkopf et al. \(2021\)](#), which allows dependent concepts. They require interventions on the data generating process to align the learned embeddings and concepts, for which they require annotations. In contrast to our framework, these works do not provide guarantees about correctness of the learned concepts or the number of labels.

We draw heavily on the field of Causal Representation Learning (CRL) ([Schölkopf et al., 2021](#)). This area assumes that there is an underlying unobserved causal system with causal variables and for each state of this system, we can only observe an entangled measurement or observation of the variables, which we say is produced by a *mixing function*. The task is then to recover the latent causal variables from the observation by learning an *unmixing* function. It can be shown that recovering these latent variables is only possible up to a permutation and transformation, which is typically element-wise for each variable. Many CRL methods exist with different assumptions on the available data, e.g. the availability of interventional, counterfactual or temporal data, or parametric assumptions on the underlying system and mixing function, e.g. (non) Gaussianity of the causal variables or (piecewise) linearity of the mixing function, and different types of identifiability guarantees, e.g. ([Hyvärinen et al., 2019](#); [Khemakhem et al., 2020](#); [von Kügelgen et al., 2021](#); [Lachapelle et al., 2022](#); [Lippe et al., 2022](#); [Ahuja et al., 2023](#); [Lachapelle et al., 2024](#); [Yao et al., 2024](#)) and many others. Our work is agnostic to which CRL method one is using, and instead focuses on the downstream task of aligning concepts efficiently to the causal representations based on general identifiability guarantees.

3 Framework and Main Definitions

Our setting takes inspiration from causal representation learning (CRL) [Schölkopf et al. \(2021\)](#) and the connections between CRL and concept-based models described by [Marconato et al. \(2022, 2023\)](#). As illustrated in Figure 2, we assume that the underlying causal system consists of several unobserved random variables: the *causal variables* $G = (G_1, \dots, G_d) \in \mathcal{G} \subseteq \mathbb{R}^d$, which can potentially have causal relations between them. The *observation* is denoted by $X \in \mathcal{X} \subseteq \mathbb{R}^D$ and is generated by an unobserved mixing function $f: \mathcal{G} \rightarrow \mathcal{X}$, possibly with additive noise ε :

$$X = f(G) + \varepsilon, \quad (f \text{ invertible onto its image}).$$

The goal of CRL is to identify the causal variables by learning an unmixing function $g_\psi: \mathcal{X} \rightarrow \mathbb{R}^d$ that approximates f^{-1} , but usually only up to a permutation and element-wise transformations. We denote the learned causal variables as $M = (M_1, \dots, M_d) \in \mathbb{R}^d$. For simplicity of exposition, in the main paper we will assume that the human interpretable concepts $C = (C_1, \dots, C_d)^\top \in \mathbb{R}^d$ that we are interested in, correspond to the ground truth causal variables G_1, \dots, G_d up to permutation and element-wise transformations, or in other words g_ψ shown in Figure 2 also identifies ground truth causal variables. In Appendix A and Section 5 this is extended to allow each of the concepts to be a transformation of a group of causal variables. Our goal is to learn the alignment map α that transforms the learned representations M to the concepts C efficiently and accurately.

In order to formalize our setting, we will need to introduce some concepts from CRL. A parametric model class $\mathcal{P} = \{P_\theta: \theta \in \Theta\}$ is called *identifiable* if the map from the parameter θ to the model P_θ is injective. In CRL, identifiability of the unmixing function is often too much to ask for, as there are often many unmixing functions that result in the same observational distribution. What is possible, and can still be useful in practical settings, is *identifiability up to an equivalence class*. Let \sim denote an equivalence relation on the space Θ . Then, θ is *identifiable up to \sim* if

$$P_\theta(X) = P_{\theta'}(X) \implies \theta \sim \theta'.$$

The equivalence class Θ/\sim is also called an *identifiability class*. Intuitively this identifiability class describes up to which transformations we can recover the ground truth variables under the appropriate assumptions.

Definition 3.1. Two models (f, P) and (g, Q) are equivalent according to \sim , if $P = Q$ and there exists an invertible matrix $A \in \mathbb{R}^{d \times d}$ and a element-wise transformation $T(z) = (T_1(z_1), \dots, T_d(z_d))^\top$ such that

$$f^{-1}(x) = AT(g^{-1}(x)) \text{ for all } x \in \mathcal{X} \subseteq \mathbb{R}^D.$$

If A is a (block)-permutation matrix then we denote the relation by $\overset{P}{\sim}$ and A is often replaced by P .

A common version of Definition 3.1 is that the model is identifiable up to a scaling and permutation, which is described by T being a diagonal scalar matrix (Hyvärinen et al., 2023). In other settings, the transformation is often a diffeomorphism and in some cases the causal variables can be either multidimensional Lippe et al. (2022) or they can only be identified up to a *block*, i.e. a group of causal variables (Ahuja et al., 2023; von Kügelgen et al., 2021; Yao et al., 2024; Lachapelle et al., 2024). For our theoretical analysis, we assume that we are given an unmixing function g_ψ from a CRL method that perfectly identifies the causal variables up to Definition 3.1 and that the human-interpretable concepts are also a result of another unknown unmixing function $g'_{\psi'}$.

Assumption 3.2. We are given a model $g_\psi: \mathcal{X} \rightarrow \mathbb{R}^d$, that is a diffeomorphism onto its image, such that $g_\psi \overset{P}{\sim} f^{-1}$, where f is the true mixing function. The unknown function $g'_{\psi'}$ that recovers the concepts C is also $g'_{\psi'} \overset{P}{\sim} f^{-1}$.

This assumption means that both the representations learned by a CRL method M and the human interpretable concepts C identify the ground truth causal variables G up to $\overset{P}{\sim}$, and the relation between M and C is also up to the same equivalence. More formally, let $\pi: \{1, \dots, d\} \rightarrow \{1, \dots, d\}$ be a permutation of the variable indices. Let $P \in \mathbb{R}^{d \times d}$ be the permutation matrix associated with π , meaning that $P_{i\pi(i)} = 1$ and 0 otherwise, and T a map as in Definition 3.1, then M and C are related by

$$PT(M) = \begin{bmatrix} T_{\pi(1)}(M_{\pi(1)}) \\ T_{\pi(2)}(M_{\pi(2)}) \\ \vdots \\ T_{\pi(d)}(M_{\pi(d)}) \end{bmatrix} = \begin{bmatrix} C_1 \\ C_2 \\ \vdots \\ C_d \end{bmatrix} = C. \tag{1}$$

Finding the α in Figure 2 reduces to learning the permutation π and a separate regression per concept C_i to learn the transformation from machine variable $M_{\pi(i)}$ to C_i . If we had access to the permutation, this would be

Algorithm 1 Estimating the permutation using linear regression with Group Lasso regularization

- 1: Input: regularization parameter $\lambda > 0$
- 2: Data: $\{(C^{(\ell)}, M^{(\ell)})\}_{\ell=1}^n$
- 3: **for** $i = 1, \dots, d$ **do**
- 4: $\hat{\beta}_i \leftarrow \arg \min_{\beta \in \mathbb{R}^{dp}} \|C_i - \Phi\beta\|^2 + \lambda\sqrt{p}\|\beta\|_{2,1}$
- 5: **end for**
- 6: $\hat{\pi} \leftarrow \arg \max_{\pi \in \Pi} \sum_{i=1}^d \|\hat{\beta}_i^{\pi(i)}\|$

a standard regression problem. What is less well studied is identifying π from observational data, i.e. without performing interventions. In the following we introduce two estimators for this setting, one assuming the element-wise transformation is linear, e.g. as is the case in some CRL methods like [Hyvärinen et al. \(2019\)](#); [Khemakhem et al. \(2020\)](#), for which we will be able to provide finite sample results based on a tunable parameters, and a second, non-parametric method based on kernel methods that allows for arbitrary invertible element-wise transformations, and can hence be applied to most CRL methods. For the second approach we will only be able to provide asymptotic results, which tell the practitioner how the regularization parameter has to scale given the number of data points. We show in the experiments that both methods work well in the low data regime and when the data is not even fully disentangled, so violating Assumption 3.2.

4 Linear Regression Permutation Learning with the Group Lasso

In this section, we describe a linear regression approach based on the Group Lasso to learn the permutation π and transformation T in (1). The approach is summarized in Algorithm 1. We will prove that this method simultaneously provides accurate regression estimates for T and identifies π correctly with high probability. To simplify the exposition, we focus here on the case of scalar variables. Proofs are in Appendix A, which also contains discussion of the assumptions, and a generalization to block variables. The proof combines techniques from high-dimensional statistics ([Bühlmann and Van De Geer, 2011](#); [Lounici et al., 2011](#)).

4.1 Method

Linear regression can describe non-linear relations by transforming covariates using a feature map $\varphi : \mathbb{R} \rightarrow \mathbb{R}^p$. In this section, we assume that T_i can be expressed as a linear function of $\varphi(M_{\pi(i)})$. The choice of φ therefore gives precise control to trade off interpretability with expressive power for T_i . For instance, in the simplest and most easily interpretable case, φ can be the identity function, so that $p = 1$ and C_i and $M_{\pi(i)}$ are related by scaling. In more challenging settings, richer functional relations may be needed, e.g. splines or random Fourier features. We apply the same feature map to all machine variables in M , for which we write $\varphi(M) = [\varphi(M_1)^\top, \dots, \varphi(M_d)^\top]^\top$. Then each C_i is modeled as a linear function of the transformed variables:

$$C_i = \varphi(M)\beta_i^* + \varepsilon_i, \tag{2}$$

where $\beta_i^* \in \mathbb{R}^{pd}$ is an unknown parameter vector, and $\varepsilon_i \sim \mathcal{N}(0, \sigma^2)$ is Gaussian noise. By assumption, C_i only depends on $M_{\pi(i)}$ and not on any of the other variables, so β_i^* is sparse: only the coefficients for $\varphi(M_{\pi(i)})$ are non-zero. To express this formally, let $G_j = \{(j-1)p, \dots, jp\}$ be the indices that belong to variable M_j and, for any $\beta \in \mathbb{R}^{pd}$, define $\beta^j = (\beta_k \mid k \in G_j)$ to be the corresponding coefficients. Then $(\beta_i^*)^j$ is non-zero only for $j = \pi(i)$.

We assume we are given a data set $\mathcal{D} = \{(C^{(\ell)}, M^{(\ell)})\}_{\ell=1}^n$ that contains n independent samples of corresponding pairs $C^{(\ell)} = (C_1^{(\ell)}, \dots, C_d^{(\ell)})$ and $M^{(\ell)} = (M_1^{(\ell)}, \dots, M_d^{(\ell)})$. We stack the $C^{(\ell)}$ into a matrix $\mathbf{C} \in \mathbb{R}^{n \times d}$

and the feature vectors $\varphi(M^{(\ell)})$ into $\Phi \in \mathbb{R}^{n \times pd}$. This leads to the relation

$$\mathbf{C}_i = \Phi \beta_i^* + \varepsilon_i,$$

where \mathbf{C}_i is the i -th column of \mathbf{C} and the noise vector ε_i consists of n independently drawn $\mathcal{N}(0, \sigma^2)$ variables. To estimate β_i^* , we use the Group Lasso with parameter $\lambda > 0$:

$$\widehat{\beta}_i = \arg \min_{\beta \in \mathbb{R}^{dp}} \frac{1}{n} \|\mathbf{C}_i - \Phi \beta\|^2 + \lambda \sqrt{p} \|\beta\|_{2,1}. \quad (3)$$

The $(2, 1)$ -mix norm $\|\beta\|_{2,1}$ in (4) encourages group-wise sparsity. It applies the Euclidean norm $\|\beta^j\|$ to each group j separately, and sums the results over groups, as defined below. We also define the $(2, \infty)$ -mix norm:

$$\|\beta\|_{2,1} = \sum_{j=1}^d \|\beta^j\|, \quad \|\beta\|_{2,\infty} = \max_{j=1,\dots,d} \|\beta^j\|. \quad (4)$$

4.2 Theoretical Analysis

We denote the full covariance matrix by $\widehat{\Sigma} = \frac{1}{n} \Phi^\top \Phi$. For the group of p columns of Φ that correspond to $\varphi(M_j)$ we write $\Phi_j = \Phi_{G_j}$. Also let $\widehat{\Sigma}_{jj'} = \frac{1}{n} \Phi_j^\top \Phi_{j'}$ denote the covariance matrix between groups j and j' , and abbreviate $\widehat{\Sigma}_j = \widehat{\Sigma}_{jj}$. Then, w.l.o.g., we can assume that the data within each group have been centered and decorrelated:

$$\frac{1}{n} \mathbb{1}^\top \Phi_j = 0 \quad \text{and} \quad \widehat{\Sigma}_j = I \quad \text{for all } j = 1, \dots, d. \quad (5)$$

This can be achieved by pre-processing: subtract the empirical mean of Φ_j and multiply it from the right by the inverse square root of the empirical covariance matrix. Preprocessing is allowed in our theoretical results, because they apply to the fixed design setting, so probabilities refer to the randomness in \mathbf{C} conditional on already having observed Φ . If $\varphi(M_j)$ and $\varphi(M_{j'})$ are completely correlated, then β_i^* is not uniquely identifiable, no matter how much data we have. To rule out this possibility, we make the following assumption, which limits the amount of correlation:

Assumption 4.1. There exists $a > 1$ s.t. for all $j \neq j'$,

$$\max_{t \in \{1, \dots, p\}} |(\widehat{\Sigma}_{jj'})_{tt}| \leq \frac{1}{14a}, \quad \max_{t, t' \in \{1, \dots, p\}} |(\widehat{\Sigma}_{jj'})_{tt'}| \leq \frac{1}{14ap}.$$

Theorem 4.2. Suppose the data have been pre-processed to satisfy (5) and let Assumption (4.1) hold. Take $\lambda \geq 4\lambda_0$, where

$$\lambda_0 = \frac{2\sigma}{\sqrt{n}} \sqrt{1 + \sqrt{\frac{8 \log(d/\delta)}{p}} + \frac{8 \log(d/\delta)}{p}},$$

and set $c = \left(1 + \frac{24}{7(a-1)}\right)$. Then, for any $\delta \in (0, 1)$, any solution $\widehat{\beta}_i$ of the Group Lasso objective (3) satisfies

$$\|\widehat{\beta}_i - \beta_i^*\|_{2,\infty} \leq c\lambda\sqrt{p} \quad (6)$$

with probability at least $1 - \frac{\delta}{d}$.

If, in addition, $\|(\beta_i^*)^{\pi(i)}\| > 2c\lambda\sqrt{p}$, then (6) implies that

$$\widehat{J}_i = \arg \max_{j=1,\dots,d} \|\widehat{\beta}_i^j\|$$

estimates $\pi(i)$ correctly.

Algorithm 2 Estimating the permutation using kernels

- 1: Input: reg. parameter $\lambda > 0$, kernels $\kappa_1, \dots, \kappa_d$
 - 2: Data: $\{(C^{(\ell)}, M^{(\ell)})\}_{\ell=1}^n$
 - 3: **for** $j = 1, \dots, d$ **do**
 - 4: $(K_j)_{\ell k} \leftarrow \kappa_j(M^{(\ell)}, M^{(k)})$
 - 5: $L_j \leftarrow \text{CholeskyDecomposition}(K_j)$
 - 6: **end for**
 - 7: **for** $i = 1, \dots, d$ **do**
 - 8: $\hat{\gamma}_i \leftarrow \arg \min_{\gamma \in \mathbb{R}^{n \times p}} \frac{1}{n} \|\mathbf{C}_i - \sum_{j=1}^d L_j \gamma^j\|^2 + \lambda \|\gamma\|_{2,1}$
 - 9: **end for**
 - 10: $\hat{\pi} \leftarrow \arg \max_{\pi \in \Pi} \sum_{i=1}^d \|\hat{\gamma}_i^{\pi(i)}\|$
-

Theorem 4.2 gives us an explicit relation between the parameters n, p, d, δ of the learning task, the tuning of the hyperparameter λ , and the estimation errors for β_i^* and $\pi(i)$. For example, if we set $\delta = \frac{1}{n}$, $\lambda = 4\lambda_0$ and let $n \rightarrow \infty$, then $\lambda \rightarrow 0$ and \hat{J}_i estimates the correct index $\pi(i)$ with probability tending to 1. So, regardless of the true parameter magnitude $\|(\beta_i^*)^{\pi(i)}\|$, the estimator is consistent given a sufficient amount of data. Another way to express this is to ask about *sample complexity*: which sample size n do we need to reach accuracy $E > 0$? Setting $\lambda = 4\lambda_0$ and solving for n large enough that $c\lambda\sqrt{p} \leq E$, we see that

$$n \geq \frac{64c^2\sigma^2(p + \sqrt{8p \log(d/\delta)}) + 8 \log(d/\delta)}{E^2}$$

is sufficient. For estimating the permutation $\pi(i)$ correctly, the required accuracy is $E \leq \|(\beta_i^*)^{\pi(i)}\|/2$, so the larger the true parameters, the easier this task becomes.

The estimation is performed separately for each concept C_i , and, if \hat{J}_i is correct for all i simultaneously, we can construct a valid estimate of the permutation by $\tilde{\pi}(i) = \hat{J}_i$. However, this estimate is not robust to estimation errors and may even produce functions $\tilde{\pi}$ that are not permutations if some \hat{J}_i are incorrect. The actual estimator of the permutation, $\hat{\pi}$, therefore optimizes a weighted matching problem, which leads to the same estimate as $\tilde{\pi}$ if the \hat{J}_i together produce a valid permutation, but forces $\hat{\pi}$ to be a valid permutation even if they do not:

$$\hat{\pi} = \arg \max_{\pi \in \Pi} \sum_{i=1}^d \|\hat{\beta}_i^{\pi(i)}\|. \tag{7}$$

Here, Π is the set of all permutations. This assignment can be solved without cycling through all permutations, with has cubic runtime in the dimension d . By a union bound over i , it follows from Theorem 4.2 that $\hat{\pi}$ estimates the true permutation π with high probability:

Corollary 4.3. *Assume the same setting as Theorem 4.2 such that for each $i = 1, \dots, d$, $\|(\beta_i^*)^{\pi(i)}\| > 2c\lambda\sqrt{p}$ and consider the estimator $\hat{\pi}$ as defined in (7). Then $\hat{\pi} = \pi$ with probability at least $1 - \delta$.*

5 Kernelized Permutation Learning

The previous section describes how to learn functions with finite-dimensional representations. We now extend the estimator to use general functions from a *Reproducing Kernel Hilbert Space* (RKHS) (Hofmann et al., 2008). This may be interpreted as a (typically infinite-dimensional) feature map φ that maps to the RKHS. However, using a representer theorem, all operations can be performed on finite-dimensional representations. We summarize the method in Algorithm 2.

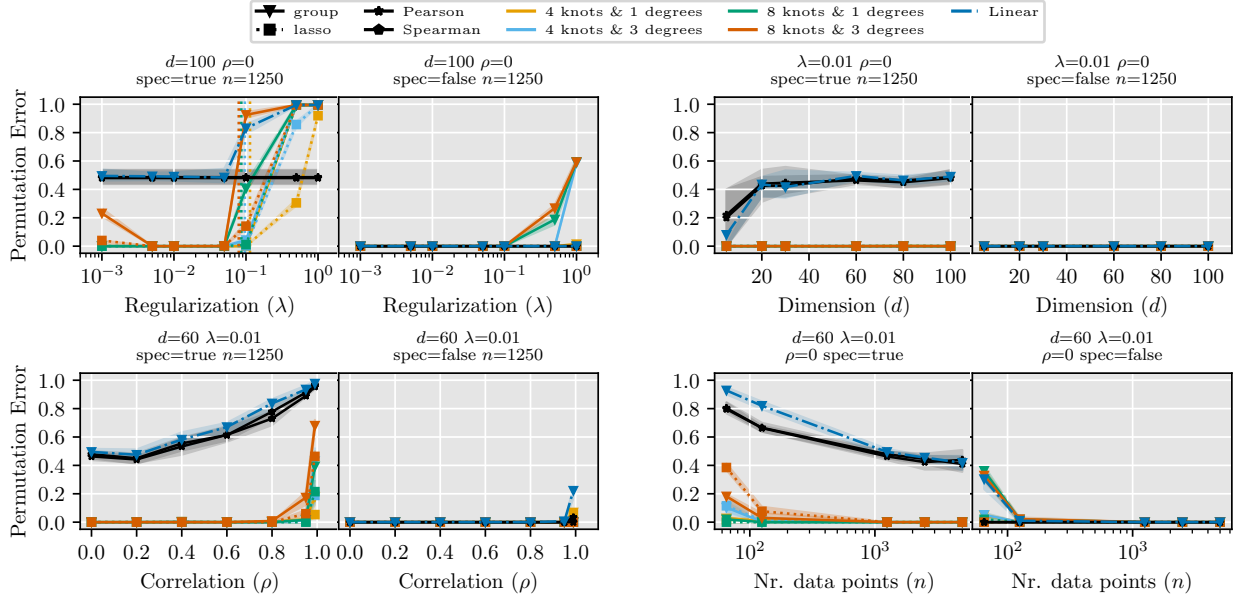


Figure 3: Permutation error rate for spline features. From top left to bottom right we vary: (i) the regularization parameter, (ii) the number of dimensions, (iii) the correlation of the variables and (iv) the number of labels. The first plot of each pair shows the wellspecified and the second the misspecified case. We average over 10 seeds and shade the 25-75th percentile.

5.1 Method

Define again $M = (M_1, \dots, M_d)$, where we now allow each machine variable M_j to take values in an abstract space \mathcal{Z}_j . Let $\mathcal{Z} = \mathcal{Z}_1 \times \dots \times \mathcal{Z}_d$. We then generalize (2) to

$$C_i = \beta_i^*(M) + \varepsilon_i,$$

where $\beta_i^* \in \mathcal{H}$ is a function from \mathcal{Z} to \mathbb{R} , and $\varepsilon_i \sim \mathcal{N}(0, \sigma^2)$. We take the space of possible functions \mathcal{H} to be an RKHS containing functions of the form $\beta(M) = \sum_{j=1}^d \beta^j(M_j)$, where each β^j is an element of an RKHS \mathcal{H}_j that captures the effect of variable M_j on C_i . The assumption that C_i depends only on $M_{\pi(i)}$ means that $\beta_i^*(M) = (\beta_i^*)^{\pi(i)}(M_{\pi(i)})$. Each \mathcal{H}_j can be freely chosen, and is typically specified indirectly by the choice of a positive definite kernel $\kappa_j : \mathcal{Z}_j \times \mathcal{Z}_j \rightarrow \mathbb{R}$ (Hofmann et al., 2008). This kernel defines a measure of similarity between inputs: $\kappa_j(M_j, M'_j) = \langle \varphi_j(M_j), \varphi_j(M'_j) \rangle_{\mathcal{H}_j}$, where $\varphi_j : \mathcal{Z}_j \rightarrow \mathcal{H}_j$ is the corresponding feature map. See p. 28 for examples.

Given data $\mathcal{D} = \{(C^{(\ell)}, M^{(\ell)})\}_{\ell=1}^n$, let $\mathbf{M} \in \mathcal{Z}^n$ denote the matrix with the machine variables $(M^{(\ell)})^\top$ stacked as rows. If we further define $\beta(\mathbf{M}) = [\beta(M^{(1)}), \dots, \beta(M^{(\ell)})]^\top$, then the Group Lasso objective (3) generalizes to

$$\hat{\beta}_i = \arg \min_{\beta \in \mathcal{H}} \frac{1}{n} \|\mathbf{C}_i - \beta(\mathbf{M})\|^2 + \lambda \sum_{j=1}^d \|\beta^j\|_{\mathcal{H}_j}, \quad (8)$$

where $\|\beta^j\|_{\mathcal{H}_j}$ is the norm associated with \mathcal{H}_j .

To optimize the objective in (8), we need a finite dimensional objective to give to a Group Lasso solver. We provide a version of the Representer Theorem showing that the solution of (8) lives in a subspace of \mathcal{H} that can be described by finite-dimensional parameters $\hat{c}_i^1, \dots, \hat{c}_i^d \in \mathbb{R}^n$:

Theorem 5.1. *Let $\varphi_1, \dots, \varphi_d$ be the feature maps associated with $\mathcal{H}_1, \dots, \mathcal{H}_d$. Then there exist $\hat{c}_i^1, \dots, \hat{c}_i^d \in \mathbb{R}^n$ such that the optimization problem in (8) has solution $\hat{\beta}_i$ with each $\hat{\beta}_i^j$ of the form*

$$\hat{\beta}_i^j = \sum_{\ell=1}^n \varphi_j(M_j^{(\ell)})(\hat{c}_i^j)_\ell.$$

Substitution of this form into (8) gives that $\hat{c}_i^1, \dots, \hat{c}_i^d$ will be the minimizers of the following finite-dimensional optimization problem:

$$\min_{c^1, \dots, c^d \in \mathbb{R}^n} \frac{1}{n} \|\mathbf{C}_i - \sum_{j=1}^d K_j c^j\|^2 + \lambda \sum_{j=1}^d \|c^j\|_{K_j}, \quad (9)$$

where $K_j \in \mathbb{R}^{n \times n}$ denotes the Gram matrix K_j , with $(K_j)_{\ell k} = \kappa_j(M_j^{(\ell)}, M_j^{(k)})$, and $\|c^j\|_{K_j} = \sqrt{c^{j \top} K_j c^j}$.

This procedure is then performed for $i = 1, \dots, d$. The permutation is estimated similarly to the linear case:

$$\hat{\pi} = \arg \max_{\pi \in \Pi} \sum_{i=1}^d \|\hat{c}_i^{\pi(i)}\|_{K_{\pi(i)}}.$$

5.2 Theoretical Analysis

Using a result by [Bach \(2008\)](#), we can prove that our estimator for π is consistent under suitable conditions, which are discussed in [Appendix B](#). This result holds for random design, so for the joint randomness of \mathcal{D} .

Theorem 5.2. *Assume (A–D) in [Appendix B.2](#). Then, for any sequence of regularization parameters λ_n such that $\lambda_n \rightarrow 0$ and $\sqrt{n}\lambda_n \rightarrow +\infty$ when $n \rightarrow \infty$, the estimated permutation $\hat{\pi}$ converges in probability to π .*

5.3 Implementation

To use a standard Group Lasso solver we need to reparametrize the optimization problem in (9), because of the scaled norms $\|\cdot\|_{K_j}$. We can do this with a Cholesky decomposition:

Lemma 5.3. *For each $j = 1, \dots, d$ let L_j be the Cholesky decomposition of the Gram matrix K_j and let $\hat{\gamma}_i^1, \dots, \hat{\gamma}_i^d$ be minimizers of*

$$\min_{\gamma^1, \dots, \gamma^d \in \mathbb{R}^n} \frac{1}{n} \|\mathbf{C}_i - \sum_{j=1}^d L_j \gamma^j\|^2 + \lambda \|\gamma^j\|_{2,1}. \quad (10)$$

Then $\hat{c}_i^j = (L_j^\top)^{-1} \hat{\gamma}_i^j$.

6 Experiments

We perform three sets of experiments to evaluate our estimators. First, we focus on a completely synthetic setting, called ‘‘Toy dataset’’. Here the concepts are generated using either a linear combination of features (which we call the wellspecified case) or diffeomorphisms (which we call the misspecified case) of the representations. The concepts are then permuted. We then evaluate the alignment of the representations learned by several state-of-the-art CRL methods to the ground truth causal variables. We look at two synthetic datasets from [Lachapelle et al. \(2022\)](#) and compare the alignment of representations learned by DMS-VAE ([Lachapelle et al., 2022](#)), iVAE ([Khemakhem et al., 2020](#)) and TCVAE ([Chen et al., 2018](#)). Finally, we evaluate on an

image benchmark, Temporal Causal3Dident (Lippe et al., 2022), comparing the alignment of representations learned by iVAE and CITRIS-VAE (Lippe et al., 2022). All experimental details are in Appendix D and our code is publicly available²

Table 1: Permutation Errors and R^2 -scores. The permutation error is bounded between 0 and 1, where 0 indicates a perfect score. For the R^2 -score, on the diagonal refers to the average score between the learned causal variable and the ground truth causal variable. The optimal score is 1. We average over 50 seeds and we write the best method in **bold**.

Model	Method	Permutation Error \downarrow (n)					R^2 -score on the diagonal \uparrow (n)				
		10	20	100	1000	10000	10	20	100	1000	10000
Action Sparsity Dataset											
DMS-VAE	NN	0.03 \pm 0.01	0.01 \pm 0.01	0.00 \pm 0.00	0.00 \pm 0.00	0.00 \pm 0.00	0.56 \pm 0.01	0.68 \pm 0.00	0.78 \pm 0.00	0.79 \pm 0.00	0.79 \pm 0.00
	Spearman	0.06 \pm 0.02	0.02 \pm 0.01	0.00 \pm 0.00	0.00 \pm 0.00	0.00 \pm 0.00	-	-	-	-	-
	Linear	0.03 \pm 0.01	0.00 \pm 0.00	0.00 \pm 0.00	0.00 \pm 0.00	0.00 \pm 0.00	0.56 \pm 0.02	0.72 \pm 0.00	0.77 \pm 0.00	0.77 \pm 0.00	0.77 \pm 0.00
	Spline	0.28 \pm 0.03	0.02 \pm 0.01	0.00 \pm 0.00	0.00 \pm 0.00	0.00 \pm 0.00	0.08 \pm 0.02	0.53 \pm 0.01	0.78 \pm 0.00	0.78 \pm 0.00	0.79 \pm 0.00
	Laplacian	0.28 \pm 0.03	0.03 \pm 0.01	0.00 \pm 0.00	0.00 \pm 0.00	0.00 \pm 0.00	-0.03 \pm 0.02	0.33 \pm 0.01	0.64 \pm 0.01	0.70 \pm 0.00	0.70 \pm 0.00
iVAE	NN	0.72 \pm 0.02	0.53 \pm 0.02	0.38 \pm 0.02	0.24 \pm 0.01	0.20 \pm 0.00	-0.14 \pm 0.03	0.10 \pm 0.01	0.29 \pm 0.00	0.31 \pm 0.00	0.31 \pm 0.00
	Spearman	0.65 \pm 0.02	0.54 \pm 0.02	0.32 \pm 0.03	0.21 \pm 0.02	0.22 \pm 0.03	-	-	-	-	-
	Linear	0.56 \pm 0.02	0.41 \pm 0.02	0.20 \pm 0.03	0.02 \pm 0.01	0.00 \pm 0.00	-0.10 \pm 0.02	0.14 \pm 0.01	0.25 \pm 0.00	0.27 \pm 0.00	0.28 \pm 0.00
	Spline	0.77 \pm 0.02	0.61 \pm 0.02	0.32 \pm 0.02	0.12 \pm 0.02	0.00 \pm 0.00	-0.18 \pm 0.02	0.05 \pm 0.01	0.24 \pm 0.00	0.27 \pm 0.00	0.27 \pm 0.00
	Laplacian	0.78 \pm 0.02	0.65 \pm 0.02	0.34 \pm 0.02	0.03 \pm 0.01	0.00 \pm 0.00	-0.23 \pm 0.02	-0.05 \pm 0.01	0.12 \pm 0.00	0.17 \pm 0.00	0.17 \pm 0.00
Temporal Causal3Dident Dataset											
CITRIS-VAE	NN	0.37 \pm 0.03	0.11 \pm 0.02	0.00 \pm 0.00	0.00 \pm 0.00	0.00 \pm 0.00	-0.17 \pm 0.04	0.22 \pm 0.02	0.42 \pm 0.01	0.59 \pm 0.00	0.65 \pm 0.00
	Spearman	0.65 \pm 0.02	0.47 \pm 0.03	0.17 \pm 0.02	0.07 \pm 0.02	0.01 \pm 0.00	-	-	-	-	-
	Linear	0.49 \pm 0.02	0.34 \pm 0.02	0.03 \pm 0.01	0.00 \pm 0.00	0.00 \pm 0.00	-0.35 \pm 0.14	0.16 \pm 0.01	0.38 \pm 0.00	0.43 \pm 0.00	0.44 \pm 0.00
	Spline	0.64 \pm 0.02	0.35 \pm 0.02	0.01 \pm 0.00	0.00 \pm 0.00	0.00 \pm 0.00	-0.33 \pm 0.08	0.09 \pm 0.01	0.40 \pm 0.00	0.52 \pm 0.00	0.55 \pm 0.00
	Laplacian	0.61 \pm 0.02	0.44 \pm 0.01	0.15 \pm 0.02	0.00 \pm 0.00	0.00 \pm 0.00	-0.37 \pm 0.09	-0.04 \pm 0.01	0.31 \pm 0.00	0.47 \pm 0.00	0.49 \pm 0.00
iVAE	NN	0.46 \pm 0.03	0.29 \pm 0.02	0.00 \pm 0.00	0.00 \pm 0.00	0.00 \pm 0.00	-0.23 \pm 0.05	0.13 \pm 0.02	0.62 \pm 0.00	0.71 \pm 0.00	0.74 \pm 0.00
	Spearman	0.55 \pm 0.03	0.36 \pm 0.02	0.08 \pm 0.02	0.00 \pm 0.00	0.00 \pm 0.00	-	-	-	-	-
	Linear	0.45 \pm 0.03	0.24 \pm 0.03	0.00 \pm 0.00	0.00 \pm 0.00	0.00 \pm 0.00	-0.20 \pm 0.03	0.14 \pm 0.01	0.43 \pm 0.00	0.47 \pm 0.00	0.48 \pm 0.00
	Spline	0.62 \pm 0.03	0.41 \pm 0.03	0.02 \pm 0.01	0.00 \pm 0.00	0.00 \pm 0.00	-0.41 \pm 0.15	0.01 \pm 0.01	0.43 \pm 0.00	0.55 \pm 0.00	0.56 \pm 0.00
	Laplacian	0.49 \pm 0.03	0.32 \pm 0.03	0.01 \pm 0.01	0.00 \pm 0.00	0.00 \pm 0.00	-0.24 \pm 0.03	0.00 \pm 0.01	0.34 \pm 0.01	0.49 \pm 0.00	0.51 \pm 0.00

Performance Metrics To assess our estimator we report the mean error in the learned permutation of the variables, $MPE = \frac{1}{d} \sum_{i=1}^d \mathbb{1}\{\tilde{\pi}(i) \neq \pi(i)\}$, the average R^2 -score of the prediction in each dimension, and the runtime.

Toy Dataset The synthetic data experiments consist of 4 settings, each using a different set of features to perform the regression. The settings are linear, splines, random Fourier features and kernels. The M variables are distributed according to $\mathcal{N}(0, (1 - \rho)I_{d \times d} + \rho \mathbb{1})$, where $\mathbb{1}$ denotes a matrix filled with only 1's. The $\rho \in (0, 1)$ parameter controls the amount of correlation between the marginal variables. We sample n data points, on which we perform a 80/20 train/test data split. In the wellspecified case we generate the M variables by using the features from that setting. For each dimension $j = 1, \dots, d$, we draw a random weight vector $\beta_j^* \in \mathbb{R}^p$, such that $\|\beta_j^*\| \in [16\lambda_0, 32\lambda_0]$ uniformly. A permutation $\pi: \{1, \dots, d\} \rightarrow \{1, \dots, d\}$ is sampled uniformly from all possible permutations. Finally, with independent $\varepsilon_i \sim N(0, \sigma^2)$ noise variables we get

$$C_i = \varphi(M_{\pi(i)})^\top \beta_{\pi(i)}^* + \varepsilon_i.$$

The misspecified case is inspired by the most general identifiability classes. In this setting the M variables are still sampled the same as in the wellspecified case, but the C variables are generated by sampling a diffeomorphism for each dimension. These outcomes are then permuted using a random permutation again. In the experiments we cover a large range of the possible values of ρ, d, n and λ as shown in Appendix D.1. Each experiment is repeated 10 times to estimate confidence bounds around the mean metric. As baseline, we compare to permutations that one can learn with Pearson or Spearman correlation. Using these correlations, we can construct a weight matrix like in our estimator and use the linear sum assignment approach to estimate

²<https://github.com/HiddeFok/sample-efficient-learning-of-concepts>

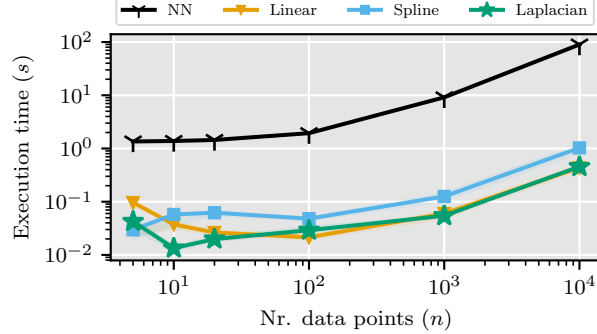


Figure 4: Execution times of the baseline and multiple versions of our estimator of learned causal representations and concepts based on the Action/Temporal Sparsity Dataset.

the permutation. This is a fast approach, but one still needs to perform a regression afterwards, while our estimator does the permutation and regression jointly, and provides correctness guarantees.

We show a set of representative results in Figure 3. Our estimator is able to reconstruct the correct permutation perfectly with only a small number of features. It performs well for a broad range of regularization parameters. In the wellspecified case we calculate the λ_0 parameter and see that the estimator performs well around this value. The dimension dependence is almost negligible, which was predicted by the dimension appearing only in the log factor in Theorem 4.2. The estimator works well with relatively few data points. Finally, the estimator works even better than theory predicts, as it has a low error even when the correlation between the dimensions is quite high. More figures using random Fourier features and the kernelized approach are in Appendix D.1.

Action/Temporal Sparsity Datasets. We use the two synthetic datasets from (Lachapelle et al., 2022) that represent the action and temporal sparsity settings in a time series. These settings have 10 causal variables $z_1, \dots, z_{10} \in [-2, 2]$ with a causal structure. The mixing function is an invertible neural network with Gaussian random weights, after which the columns in the linear layers are orthogonalized to ensure injectivity. To recover the ground truth permutation, we follow Lachapelle et al. (2022) and use the test set to calculate a permutation based on Pearson correlations.

Temporal Causal3DIdent. We evaluate our methods on an image benchmark, TemporalCausal3DIdent (Lippe et al., 2022). The dataset consists of images of 3D objects, rendered in different positions, rotation and lighting. The causal variables are the position $(x, y, z) \in [-2, 2]^3$, the object rotation with two dimensions $[\alpha, \beta] \in [0, 2\pi)^2$, the hue, the background and spotlight also in $[0, 2\pi)$. The object shape is a categorical variable. We use a pretrained CITRIS-VAE encoder, which outputs a 32 dimensional latent space and a grouping of which dimensions relate to which causal variables. Although CITRIS-VAE provides the correct permutation of the groups, we ignore it and perform a random permutation on the variables. Similar to Lippe et al. (2022), we train an MLP for each of the 32 dimensions that predicts all causal variables. Based on the R^2 scores of these regressions, we learn the group assignments. Some CRL methods provide identifiability up to blocks of variables, but do not specify how these blocks correspond to the ground truth. Our estimator offers an efficient solution in these cases.

Results. A selection of results for the action sparsity dataset and temporal Causal3DIdent dataset are reported in Table 1, while the complete set of experiments is reported in Appendix D.2–D.3. We report two baselines, NN and Spearman. The method NN refers to using a trained MLP to predict all causal variables with each encoding. The R^2 -scores are then used to determine the matching. We also added the kernelized version of our estimator with the Laplacian kernel. Our estimator consistently ranks amongst the lowest MPE scores, and it still works empirically even if there is a dependence between the ground truth variables that is potentially larger than Assumption 4.1. The Spearman correlation performs well with regards to the MPE, but a separate

regression still needs to be performed, while our estimator does everything in one procedure. In terms of R^2 -score we slightly underperform against the neural network approach, but this approach requires 100x more computing time (see Figure 4). Our estimator is able to handle blocks or vectors of inputs in the results of the temporal Causal3DIdent dataset, as predicted by Theorem 4.2 in Appendix A.

7 Conclusion

We propose a framework that provides theoretical guarantees on learning of concepts in deep learning models by leveraging causal representation learning (CRL) and techniques from high-dimensional statistics. We provide two estimators that are able to recover the permutation and mapping between the learned representations and the true concepts: a linear estimator with finite sample guarantees and a non-parametric kernelized estimator with asymptotic guarantees. We test our methods on CRL benchmarks and show they perform even better than the theory predicted. Our work can be incorporated into current concept-based models, ensuring that the concepts are learned faithfully even with few labels. For future work, it would be interesting to incorporate ideas from the *causal abstraction* literature (Rubenstein et al., 2017; Geiger et al., 2021; Beckers et al., 2020) and learn hierarchies of concepts.

Acknowledgements

We thank SURFsara for the support in using the Snellius Compute Cluster. T. Van Erven was supported by the Netherlands Organization for Scientific Research (NWO) under grant number VI.Vidi.192.095.

Impact Statement

This paper presents work whose goal is to advance the field of Machine Learning. There are many potential societal consequences of our work, none of which we feel must be specifically highlighted here.

References

- Ahuja, K., Mahajan, D., Wang, Y., and Bengio, Y. (2023). Interventional causal representation learning. In *International Conference on Machine Learning, ICML*, Proceedings of Machine Learning Research. PMLR. [3](#), [4](#)
- Alain, G. and Bengio, Y. (2017). Understanding intermediate layers using linear classifier probes. In *International Conference on Learning Representations, ICLR*. [2](#)
- Alvarez-Melis, D. and Jaakkola, T. S. (2018). Towards robust interpretability with self-explaining neural networks. In *Proceedings of the 32nd International Conference on Neural Information Processing Systems, NIPS’18*, page 7786–7795, Red Hook, NY, USA. Curran Associates Inc. [2](#), [3](#)
- Bach, F. R. (2008). Consistency of the group lasso and multiple kernel learning. *Journal of Machine Learning Research*, 9(40):1179–1225. [2](#), [9](#), [22](#), [24](#)
- Bach, F. R., Jenatton, R., Mairal, J., and Obozinski, G. (2012). Optimization with sparsity-inducing penalties. *Foundations and Trends in Machine Learning*, pages 1–106. [22](#)
- Baker, C. R. (1973). Joint measures and cross-covariance operators. *Transactions of the American Mathematical Society*. [24](#)
- Beckers, S., Eberhardt, F., and Halpern, J. Y. (2020). Approximate causal abstractions. In *Uncertainty in Artificial Intelligence UAI*. PMLR. [12](#)
- Belinkov, Y. (2022). Probing classifiers: Promises, shortcomings, and advances. *Computational Linguistics*. [1](#)
- Bengio, Y., Mindermann, S., Privitera, D., Besiroglu, T., Bommasani, R., Casper, S., Choi, Y., Fox, P., Garfinkel, B., Goldfarb, D., Heidari, H., Ho, A., Kapoor, S., Khalatbari, L., et al. (2025). International ai safety report. [1](#)
- Bühlmann, P. and Van De Geer, S. (2011). *Statistics for high-dimensional data: methods, theory and applications*. Springer Science & Business Media. [2](#), [5](#), [17](#), [18](#), [26](#)
- Chen, R. T., Li, X., Grosse, R. B., and Duvenaud, D. K. (2018). Isolating sources of disentanglement in variational autoencoders. *Advances in neural information processing systems*, 31. [9](#), [30](#)
- Chen, Z., Bei, Y., and Rudin, C. (2020). Concept whitening for interpretable image recognition. *Nature Machine Intelligence*, 2(12):772–782. [2](#), [3](#)
- Gallego-Posada, J., Ramirez, J., and Erraqabi, A. (2021). Flexible learning of sparse neural networks via constrained L_0 regularization. In *NeurIPS 2021 Workshop LatinX in AI*. [29](#)
- Geiger, A., Lu, H., Icard, T., and Potts, C. (2021). Causal abstractions of neural networks. *Advances in Neural Information Processing Systems*, 34:9574–9586. [12](#)
- Ghorbani, A., Wexler, J., Zou, J. Y., and Kim, B. (2019). Towards automatic concept-based explanations. *Advances in Neural Information Processing Systems, NeurIPS*. [2](#)
- Goyal, Y., Feder, A., Shalit, U., and Kim, B. (2019). Explaining classifiers with causal concept effect (CaCE). *arXiv preprint arXiv:1907.07165*. [1](#)

- Graziani, M., Nguyen, A.-p., O'Mahony, L., Müller, H., and Andrearczyk, V. (2023). Concept discovery and dataset exploration with singular value decomposition. In *ICLR 2023 Workshop on Pitfalls of limited data and computation for Trustworthy ML*. 1
- Hofmann, T., Schölkopf, B., and Smola, A. J. (2008). Kernel methods in machine learning. *The Annals of Statistics*, 36(3):1171–1220. 7, 8
- Hyvärinen, A., Khemakhem, I., and Monti, R. P. (2023). Identifiability of latent-variable and structural-equation models: from linear to nonlinear. *arXiv preprint arXiv:2302.02672*. 4
- Hyvärinen, A., Sasaki, H., and Turner, R. E. (2019). Nonlinear ICA using auxiliary variables and generalized contrastive learning. In *International Conference on Artificial Intelligence and Statistics, AISTATS, Proceedings of Machine Learning Research*. PMLR. 3, 5
- Ismail, A. A., Adebayo, J., Bravo, H. C., Ra, S., and Cho, K. (2023). Concept bottleneck generative models. In *International Conference on Learning Representations, ICLR*. 1, 2
- Jang, E., Gu, S., and Poole, B. (2017). Categorical reparameterization with gumbel-softmax. In *International Conference on Learning Representations, ICLR*. 30
- Khajenezhad, A., Madani, H., and Beigy, H. (2021). Masked autoencoder for distribution estimation on small structured data sets. *IEEE Transactions Neural Networks Learning Systems*, 32(11). 33
- Khemakhem, I., Kingma, D. P., Monti, R. P., and Hyvärinen, A. (2020). Variational autoencoders and nonlinear ICA: A unifying framework. In *International Conference on Artificial Intelligence and Statistics, AISTATS, Proceedings of Machine Learning Research*. PMLR. 2, 3, 5, 9, 28, 30
- Kim, B., Wattenberg, M., Gilmer, J., Cai, C., Wexler, J., Viegas, F., et al. (2018). Interpretability beyond feature attribution: Quantitative testing with concept activation vectors (TCAV). In *International Conference on Machine Learning, ICML, Proceedings of Machine Learning Research*. PMLR. 1
- Kingma, D. P. and Ba, J. (2015). Adam: A method for stochastic optimization. In *International Conference on Learning Representations, ICLR*. 29, 34
- Koh, P. W., Nguyen, T., Tang, Y. S., Mussmann, S., Pierson, E., Kim, B., and Liang, P. (2020). Concept bottleneck models. In *International Conference on Machine Learning, ICML, Proceedings of Machine Learning Research*. PMLR. 1, 2
- Lachapelle, S., López, P. R., Sharma, Y., Everett, K., Priol, R. L., Lacoste, A., and Lacoste-Julien, S. (2024). Nonparametric partial disentanglement via mechanism sparsity: Sparse actions, interventions and sparse temporal dependencies. *arXiv preprint arXiv:2401.04890*. 3, 4
- Lachapelle, S., Rodriguez, P., Sharma, Y., Everett, K. E., PRIOL, R. L., Lacoste, A., and Lacoste-Julien, S. (2022). Disentanglement via mechanism sparsity regularization: A new principle for nonlinear ICA. In *First Conference on Causal Learning and Reasoning*. 2, 3, 9, 11, 28, 30
- Lippe, P., Magliacane, S., Löwe, S., Asano, Y. M., Cohen, T., and Gavves, S. (2022). CITRIS: causal identifiability from temporal intervened sequences. In *International Conference on Machine Learning, ICML, Proceedings of Machine Learning Research*. PMLR. 2, 3, 4, 10, 11, 30, 31, 32
- Lounici, K., Pontil, M., Van De Geer, S., and Tsybakov, A. B. (2011). Oracle inequalities and optimal inference under group sparsity. *The Annals of Statistics*. 5, 17, 18, 19
- Lovering, C. and Pavlick, E. (2022). Unit testing for concepts in neural networks. *Transactions of the Association for Computational Linguistics*. 1
- Maddison, C. J., Mnih, A., and Teh, Y. W. (2017). The concrete distribution: A continuous relaxation of discrete random variables. In *International Conference on Learning Representations, ICLR*. 30

- Mahinpei, A., Clark, J., Lage, I., Doshi-Velez, F., and Pan, W. (2021). Promises and pitfalls of black-box concept learning models. [1](#), [3](#)
- Marconato, E., Passerini, A., and Teso, S. (2022). Glancenets: Interpretable, leak-proof concept-based models. In *Neural Information Processing Systems, NeurIPS*. [1](#), [2](#), [3](#)
- Marconato, E., Passerini, A., and Teso, S. (2023). Interpretability is in the mind of the beholder: A causal framework for human-interpretable representation learning. *Entropy*. [2](#), [3](#)
- Margeloiu, A., Ashman, M., Bhatt, U., Chen, Y., Jamnik, M., and Weller, A. (2021). Do concept bottleneck models learn as intended? [1](#), [3](#)
- McGrath, T., Kapishnikov, A., Tomašev, N., Pearce, A., Hassabis, D., Kim, B., Paquet, U., and Kramnik, V. (2022). Acquisition of chess knowledge in alphazero. *Proceedings of the National Academy of Sciences, PNAS*. [2](#)
- Molnar, C. (2022). *Interpretable Machine Learning*. 2 edition. [1](#)
- Rubenstein, P. K., Weichwald, S., Bongers, S., Mooij, J. M., Janzing, D., Grosse-Wentrup, M., and Schölkopf, B. (2017). Causal consistency of structural equation models. In *Conference on Uncertainty in Artificial Intelligence, UAI*. AUAI Press. [12](#)
- Schölkopf, B., Herbrich, R., and Smola, A. J. (2001). A generalized representer theorem. In *International conference on computational learning theory*. Springer. [23](#)
- Schölkopf, B., Locatello, F., Bauer, S., Ke, N. R., Kalchbrenner, N., Goyal, A., and Bengio, Y. (2021). Toward causal representation learning. *Proceedings of the IEEE*. [3](#)
- von Kügelgen, J., Sharma, Y., Gresele, L., Brendel, W., Schölkopf, B., Besserve, M., and Locatello, F. (2021). Self-supervised learning with data augmentations provably isolates content from style. In *Advances in Neural Information Processing Systems, NeurIPS*. [3](#), [4](#), [31](#)
- Williams, C. and Seeger, M. (2000). Using the nyström method to speed up kernel machines. In *Advances in Neural Information Processing Systems, NeurIPS*, volume 13. MIT Press. [25](#)
- Yao, D., Xu, D., Lachapelle, S., Magliacane, S., Taslakian, P., Martius, G., von Kügelgen, J., and Locatello, F. (2024). Multi-view causal representation learning with partial observability. In *International Conference on Learning Representations, ICLR*. [3](#), [4](#)
- Yuan, M. and Lin, Y. (2006). Model selection and estimation in regression with grouped variables. *Journal of the Royal Statistical Society Series B: Statistical Methodology*. [2](#)
- Zarlenga, M. E., Barbiero, P., Ciravegna, G., Marra, G., Giannini, F., Diligenti, M., Shams, Z., Precioso, F., Melacci, S., Weller, A., et al. (2022). Concept embedding models: beyond the accuracy-explainability trade-off. In *Advances in Neural Information Processing Systems, NeurIPS*. [1](#), [2](#)
- Zimmermann, R. S., Sharma, Y., Schneider, S., Bethge, M., and Brendel, W. (2021). Contrastive learning inverts the data generating process. In *International Conference on Machine Learning, ICML*, Proceedings of Machine Learning Research. PMLR. [31](#)

A Proofs Linear Regression Approach

As discussed in Section 4, we will extend Theorem 4.2 to a more general result Theorem A.5 that allows for blocks of causal variables corresponding to a single concept. To state the general result we will redefine our model and introduce additional notation. The variables $C_i \in \mathbb{R}$ and $M_j \in \mathbb{R}^{k_j}$ now live in potentially different spaces. Let $C = (C_1, \dots, C_d)^\top \in \mathbb{R}^d$ and $M = (M_1, \dots, M_d)^\top \in \mathbb{R}^k$, where $k = \sum_{j=1}^d k_j \geq d$. Let $K_j = \{\sum_{a=1}^{j-1} k_a + b \mid b \in \{1, \dots, k_j\}\}$ denote the subset of indices in M that correspond to the block M_j . The permutation that we want to recover is π . Each dimension in the M variable can be transformed through a separate feature map $\varphi_t: \mathbb{R} \rightarrow \mathbb{R}^{p_t}$ that can be different for each $t = 1, \dots, k$. We will denote the total feature vector by

$$\varphi(M) = \begin{bmatrix} \varphi_1(M_1) \\ \vdots \\ \varphi_k(M_k) \end{bmatrix}.$$

The grouped features will be denoted by $\varphi(M)^j = (\varphi_t(M_t) \mid t \in K_j)$. Define the average feature set size as $\bar{p} = \frac{1}{k} \sum_{t=1}^k p_t$. The model is described by

$$C_i = \varphi(M)\beta_i^* + \varepsilon_i, \quad \beta_i^* \in \mathbb{R}^{k\bar{p}}, \varepsilon_i \sim \mathcal{N}(0, \sigma^2).$$

For the actual regression task, we can define data matrices again. The matrix \mathbf{C} will be defined as in the main text and Φ now becomes an $n \times k\bar{p}$ matrix, in which all feature vectors $\varphi(M^{(\ell)})$ are stacked. With ε_i denoting n independently draw $\mathcal{N}(0, \sigma^2)$ variables, this results in the relation

$$\mathbf{C}_i = \Phi\beta_i^* + \varepsilon_i.$$

The β_i^* again has a sparse structure, because only the parameters corresponding to $\varphi(M)^j$ should be non-zero. Let the indices of these parameters be denoted by G_j . Alternatively, this G_j is defined through $\varphi(M)_{G_j} = \varphi(M)^j$. Thus, in this setting we again have d groups all denoted by G_j . To ease notation we set again $\beta_i^j = ((\beta_i)_t \mid t \in G_j)$. The definitions of the norm $\|\cdot\|_{2,\infty}$ and covariance matrices, $\widehat{\Sigma}_{jj'} = \frac{1}{n} \varphi(M)_{G_j}^\top \varphi(M)_{G_{j'}} = \frac{1}{n} \Phi_j^\top \Phi_{j'}$, are altered in accordance with these groups. As the groups can now be of different size, we have to change the definition of the $\|\cdot\|_{2,1}$ -norm to take the different group sizes into account,

$$\|\beta\|_{2,1} = \sum_{j=1}^d \|\beta^j\| \sqrt{p^j},$$

where $p^j = \sum_{t \in K_j} p_t$. The loss function that we want to optimize to estimate β_i^* has the same form as before

$$\widehat{\beta}_i = \arg \min_{\beta \in \mathbb{R}^{k\bar{p}}} \frac{1}{n} \|\mathbf{C}_i - \Phi\beta\|^2 + \lambda \|\beta\|_{2,1} = \arg \min_{\beta \in \mathbb{R}^{k\bar{p}}} \frac{1}{n} \|\mathbf{C}_i - \Phi\beta\|^2 + \lambda \sum_{j=1}^d \|\beta^j\| \sqrt{p^j}. \quad (11)$$

The optimality conditions for any solution, $\widehat{\beta}_i$, for this convex optimization problem are given by

$$\frac{1}{n} (\Phi^\top (\mathbf{C}_i - \Phi\widehat{\beta}_i))^j = \frac{\lambda \sqrt{p^j}}{2} \frac{\widehat{\beta}_i^j}{\|\widehat{\beta}_i^j\|} \quad \text{if } \widehat{\beta}_i^j \neq 0, \quad (12)$$

$$\frac{1}{n} \|\Phi^\top (\mathbf{C}_i - \Phi\widehat{\beta}_i)\|^2 \leq \frac{\lambda \sqrt{p^j}}{2} \quad \text{if } \widehat{\beta}_i^j = 0. \quad (13)$$

To ensure that our results hold even in the case where $n < pd$, we introduce a standard assumption on the data from the high-dimensional statistics literature. Intuitively, this assumption ensures that the data is “variable enough” in the directions that matter.

Assumption A.1. The Restricted Eigen Value (RE(1)) is satisfied by the data matrix $\Phi \in \mathbb{R}^{n \times k\bar{p}}$ if there exists a $\kappa > 0$ such that for all $\Delta \in \mathbb{R}^{k\bar{p}} \setminus \{0\}$ and $j = 1, \dots, d$ with $\sum_{i \neq j} \|\Delta^i\| \sqrt{p^i} \leq 3\|\Delta^j\| \sqrt{p^j}$ it holds that

$$\frac{\|\Phi\Delta\|}{\sqrt{n}\|\Delta^j\|} \geq \kappa.$$

This property is satisfied for any $\Delta \in \mathbb{R}^{k\bar{p}} \setminus \{0\}$ if $\widehat{\Sigma} = \frac{1}{n}\Phi^T\Phi$ has a positive minimal eigenvalue. Let $\lambda_{\min} > 0$ be the minimal eigenvalue of $\widehat{\Sigma}$, then

$$\|\Phi\Delta\|^2 = \Delta^T\Phi^T\Phi\Delta = n\Delta^T\widehat{\Sigma}\Delta \geq n\lambda_{\min}\Delta^T\Delta = n\lambda_{\min}\|\Delta\|^2.$$

Now divide by n and take the square root on both sides. This gives us

$$\frac{\|\Phi\Delta\|}{\sqrt{n}} \geq \sqrt{\lambda_{\min}}\|\Delta\| = \sqrt{\lambda_{\min}}\sqrt{\sum_{i=1}^d \|\Delta^i\|^2} \geq \sqrt{\frac{\lambda_{\min}}{d}} \sum_{i=1}^d \|\Delta^i\| \geq \sqrt{\frac{\lambda_{\min}}{d}}\|\Delta^j\|.$$

The second inequality follows from an application of Jensen's inequality. Dividing both sides by $\|\Delta^j\|$ gives the desired result.

The matrix $\widehat{\Sigma}$ is the empirical covariance matrix and will be positive definite almost surely whenever $n \geq k\bar{p}$ and hence RE(1) will be satisfied if $n \geq k\bar{p}$.

Finally, define $p_{\min} = \min_{j=1, \dots, d} p^j$ and $p_{\max} = \max_{j=1, \dots, d} p^j$. The following theorems and proofs are adapted from Chapter 8 in [Bühlmann and Van De Geer \(2011\)](#) and sections 3 and 5 in [Lounici et al. \(2011\)](#).

Theorem A.2. Assume that for all $\ell = 1, \dots, n$, $\varepsilon_i^{(\ell)} \sim \mathcal{N}(0, \sigma^2)$ independently, $\sigma^2 > 0$, the RE(1) condition is satisfied with $\kappa > 0$ and consider the Group Lasso estimator

$$\widehat{\beta}_i = \arg \min_{\beta \in \mathbb{R}^{k\bar{p}}} \frac{1}{n} \|\mathbf{C}_i - \Phi\beta\|^2 + \lambda \|\beta\|_{2,1},$$

where $\lambda \geq 4\lambda_0$ with

$$\lambda_0 = \frac{2\sigma}{\sqrt{n}} \sqrt{1 + \sqrt{\frac{8 \log(d/\delta)}{p_{\min}}} + \frac{8 \log(d/\delta)}{p_{\min}}}.$$

Then, for any $\delta \in (0, 1)$, with probability at least $1 - \frac{\delta}{d}$,

$$\frac{1}{n} \|\mathbf{C}_i - \Phi\widehat{\beta}_i\|^2 + \lambda \|\widehat{\beta}_i - \beta_i^*\|_{2,1} \leq \frac{24\lambda^2 p^{\pi(i)}}{\kappa^2} \quad (14)$$

$$\|(\widehat{\Sigma}(\widehat{\beta} - \beta^*))^j\| \leq \lambda \sqrt{p^j} \quad \text{for all } j = 1, \dots, d \quad (15)$$

$$\|\widehat{\beta} - \beta^*\|_{2,1} \leq \frac{24\lambda p^{\pi(i)}}{\kappa^2}. \quad (16)$$

This theorem offers us a several things. Equation 14 gives us a bound on the true prediction error. The last two equations, (15, 16), are needed to prove that we find accurate parameter values using the Group Lasso approach. The fact that the last equation gives a bound in the $(2, 1)$ -norm, allows us to use a duality argument later on to provide a bound on the $(2, \infty)$ -norm of the difference between the learned and true parameter. Knowing that only one of the groups has to be non-zero combined with this uniform bound enables us to conclude that the correct group has been identified in the proof of [Theorem A.5](#).

Proof First let us define for every $j = 1, \dots, d$ the random events $\mathcal{A}_j = \{\frac{1}{n} \|(\Phi^T \varepsilon_i)^j\| \leq \frac{\lambda \sqrt{p^j}}{2}\}$ and their intersection $\mathcal{A} = \bigcap_{j=1}^d \mathcal{A}_j$. Most importantly, we see from [Lemma C.2](#) that this event has probability at least $1 - \frac{\delta}{d}$. We get the $1/d$ factor by using $\widetilde{\delta} = \frac{\delta}{d}$ in [Lemma C.2](#) and noticing that this only adds a factor of 2 in

the log terms. The first assertion (14) is true on the event \mathcal{A} and follows from the proof of Theorem 8.1 in (Bühlmann and Van De Geer, 2011) and noting that in our setting their oracle parameter is given by our β_i^* and that $\mathbf{f}_0 = \Phi\beta_i^*$.

Moving on towards (15), by the optimality condition (12) and (13) we have for each $j = 1, \dots, d$

$$\frac{1}{n} \|(\Phi(\mathbf{C}_i - \Phi\hat{\beta}))^j\| \leq \frac{\lambda\sqrt{p^j}}{2}.$$

Let us rewrite the expression in (15) into

$$\|(\widehat{\Sigma}(\hat{\beta}_i - \beta_i^*))^j\| = \frac{1}{n} \|(\Phi^\top(\Phi\hat{\beta} - \Phi\beta^*))^j\|.$$

Substituting $\Phi\beta_i^* = \mathbf{C}_i - \varepsilon_i$ into this expression gives

$$\begin{aligned} \|(\widehat{\Sigma}(\hat{\beta}_i - \beta_i^*))^j\| &\leq \frac{1}{n} \|(\Phi^\top(\Phi\hat{\beta}_i - \mathbf{C}_i))^j\| + \frac{1}{n} \|(\Phi^\top\varepsilon_i)^j\| \\ &\leq \frac{\lambda\sqrt{p^j}}{2} + \frac{\lambda\sqrt{p^j}}{2} = \lambda\sqrt{p^j}. \end{aligned}$$

Note that this inequality only holds on \mathcal{A} .

The final assertion is a direct consequence of the first,

$$\begin{aligned} \lambda\|\hat{\beta}_i - \beta_i^*\|_{2,1} &\leq \frac{1}{n} \|\Phi(\hat{\beta}_i - \beta_i^*)\|^2 + \lambda\|\hat{\beta}_i - \beta_i^*\|_{2,1} \leq \frac{24\lambda^2 p^{\pi(i)}}{\kappa^2} \\ \|\hat{\beta}_i - \beta_i^*\|_{2,1} &\leq \frac{24\lambda p^{\pi(i)}}{\kappa^2}. \end{aligned}$$

■

To state and prove the general version of Theorem 4.2 we also need to generalize Assumption 4.1.

Assumption A.3. There exists some constant $a > 1$ such that for any $j \neq j'$, it holds that

$$\max_{1 \leq t \leq \min(p^j, p^{j'})} |(\widehat{\Sigma}_{jj'})_{tt}| \leq \frac{1}{14a} \sqrt{\frac{p_{\min}}{p_{\max}}} \quad (17)$$

and

$$\max_{1 \leq t \leq p^j, 1 \leq t' \leq p^{j'}, t \neq t'} |(\widehat{\Sigma}_{jj'})_{tt'}| \leq \frac{1}{14a} \sqrt{\frac{p_{\min}}{p_{\max}}} \frac{1}{\sqrt{p^j p^{j'}}}. \quad (18)$$

The previous assumption is stronger than the RE(1) property, as shown by the following lemma:

Lemma A.4. Let Assumption A.3 be satisfied. Then RE(1) is satisfied with $\kappa = \sqrt{1 - 1/a}$.

Proof This is Lemma B.3 in (Lounici et al., 2011). ■

The following theorem is a modification of Theorem 5.1 by Lounici et al. (2011), where some adaptations are made to adjust the result to our setting.

Theorem A.5. Let Assumption (A.3) hold, for $\ell = 1, \dots, d$, $\varepsilon_i^\ell \sim \mathcal{N}(0, \sigma^2)$ independently, $\sigma^2 > 0$, and with $\delta \in (0, 1)$ set $\lambda \geq 4\lambda_0$, where

$$\lambda_0 = \frac{2\sigma}{\sqrt{n}} \sqrt{1 + \sqrt{\frac{8 \log(d/\delta)}{p_{\min}} + \frac{8 \log(d/\delta)}{p_{\min}}}}.$$

Furthermore, set $c = \left(1 + \frac{24}{7(a-1)}\right)$. Then, for any $\delta \in (0, 1)$, with probability at least $1 - \frac{\delta}{a}$, any solution $\hat{\beta}_i$ of (11) satisfies

$$\|\hat{\beta}_i - \beta_i^*\|_{2,\infty} \leq c\lambda\sqrt{p_{\max}}. \quad (19)$$

If, in addition, $\|(\beta_i^*)^{\pi(i)}\| > 2c\lambda\sqrt{p_{\max}}$, then (19) implies that

$$\widehat{J}_i = \arg \max_{j=1,\dots,d} \|\widehat{\beta}_i^j\|$$

estimates $\pi(i)$ correctly.

Proof Most of the proof is similar to the proof of Theorem 5.1 in Lounici et al. (2011). We supply a full proof for completeness and because our setting is slightly different. We will need more notation to prove this statement. Set $p_\infty = \max_{1 \leq d} p^j$ and define the extended covariance matrices $\widetilde{\Sigma}_{jj'}$ of size $p_\infty \times p_\infty$ as

$$\widetilde{\Sigma}_{jj'} = \begin{bmatrix} \widehat{\Sigma}_{jj'} & 0 \\ 0 & 0 \end{bmatrix} \text{ if } j \neq j' \text{ and } \widetilde{\Sigma}_{jj} = \begin{bmatrix} \widehat{\Sigma}_{jj} - I_{p^j \times p^j} & 0 \\ 0 & 0 \end{bmatrix} \text{ if } j = j'.$$

We also define for any $j = 1, \dots, d$ and $\Delta \in \mathbb{R}^{k\bar{p}}$ the vector $\widetilde{\Delta}^j \in \mathbb{R}^{p_\infty}$ such that

$$\widetilde{\Delta}^j = \begin{bmatrix} \Delta^j \\ 0 \end{bmatrix}.$$

Now set $\Delta = \widehat{\beta}_i - \beta_i^*$ and bound

$$\|\Delta\|_{2,\infty} = \|\widehat{\Sigma}\Delta - (\widehat{\Sigma} - I_{k\bar{p} \times k\bar{p}})\Delta\|_{2,\infty} \leq \|\widehat{\Sigma}\Delta\|_{2,\infty} + \|(\widehat{\Sigma} - I_{k\bar{p} \times k\bar{p}})\Delta\|_{2,\infty}.$$

The first term is controlled by (15) from Lemma A.2. The latter term can be bounded by noticing that only the off-diagonal elements will contribute to the norm. We can bound it using Cauchy-Schwarz:

$$\begin{aligned} \|(\widehat{\Sigma} - I_{k\bar{p} \times k\bar{p}})\Delta\|_{2,\infty} &= \max_{j=1,\dots,d} \|((\widehat{\Sigma} - I_{k\bar{p} \times k\bar{p}})\Delta)^j\| \\ &= \max_{j=1,\dots,d} \left[\sum_{t=1}^{p^j} \left(\sum_{j'=1}^d \sum_{t'=1}^{p^{j'}} (\widetilde{\Sigma}_{jj'})_{tt'} \widetilde{\Delta}_{t'}^{j'} \right)^2 \right]^{1/2} \\ &\leq \max_{j=1,\dots,d} \left[\sum_{t=1}^{p^j} \left(\sum_{j'=1}^d (\widetilde{\Sigma}_{jj'})_{tt} \widetilde{\Delta}_t^{j'} \right)^2 \right]^{1/2} \\ &\quad + \max_{j=1,\dots,d} \left[\sum_{t=1}^{p^j} \left(\sum_{j'=1}^d \sum_{t'=1, t' \neq t}^{p^{j'}} (\widetilde{\Sigma}_{jj'})_{tt'} \widetilde{\Delta}_{t'}^{j'} \right)^2 \right]^{1/2}. \end{aligned}$$

We now bound both terms separately. The first term can be bounded using an application of Assumption A.3 and then Minkowski's inequality. The Minkowski's inequality is true for L^p norms and tells us

$$\|x + y\|_p \leq \|x\|_p + \|y\|_p.$$

In our case this generalises to

$$\left[\sum_{t=1}^{p_\infty} \left(\sum_{j'=1}^d |\widetilde{\Delta}_t^{j'}| \right)^2 \right]^{1/2} = \left\| \sum_{j=1}^d \widetilde{\Delta}^j \right\| \leq \sum_{j=1}^d \|\widetilde{\Delta}^j\| \leq \frac{1}{\sqrt{p_{\min}}} \sum_{j=1}^d \sqrt{p^j} \|\Delta^j\| = \frac{1}{\sqrt{p_{\min}}} \|\widetilde{\Delta}\|_{2,1}.$$

Combining Assumption A.3 with the above inequality gives us

$$\begin{aligned}
 \max_{j=1,\dots,d} \left[\sum_{t=1}^{p_j} \left(\sum_{j'=1}^d (\tilde{\Sigma}_{jj'})_{tt} \tilde{\Delta}_t^{j'} \right)^2 \right]^{1/2} &\leq \frac{1}{14a} \sqrt{\frac{p_{\min}}{p_{\max}}} \left[\sum_{t=1}^{p_{\infty}} \left(\sum_{j'=1}^d |\tilde{\Delta}_t^{j'}| \right)^2 \right]^{1/2} \\
 &\leq \frac{1}{14a} \sqrt{\frac{p_{\min}}{p_{\max}}} \frac{1}{\sqrt{p_{\min}}} \|\tilde{\Delta}\|_{2,1} \\
 &\leq \frac{1}{14a} \sqrt{\frac{1}{p_{\max}}} \|\Delta\|_{2,1}.
 \end{aligned}$$

The second term can now be bounded by another application of Cauchy-Schwarz:

$$\begin{aligned}
 \max_{j=1,\dots,d} \left[\sum_{t=1}^{p^j} \left(\sum_{j'=1}^d \sum_{t'=1, t' \neq t}^{p^{j'}} (\tilde{\Sigma}_{jj'})_{tt'} \tilde{\Delta}_{t'}^{j'} \right)^2 \right]^{1/2} &\leq \frac{1}{14a} \sqrt{\frac{p_{\min}}{p_{\max}}} \max_{j=1,\dots,d} \left[\frac{1}{p^j} \sum_{t=1}^{p^j} \left(\sum_{j'=1}^d \sum_{t'=1}^{p^{j'}} \frac{|\tilde{\Delta}_{t'}^{j'}|}{\sqrt{p^{j'}}} \right)^2 \right]^{1/2} \\
 &\leq \frac{1}{14a} \sqrt{\frac{p_{\min}}{p_{\max}}} \sum_{j'=1}^d \sum_{t'=1}^{p^{j'}} \frac{|\tilde{\Delta}_{t'}^{j'}|}{\sqrt{p^{j'}}} \\
 &\leq \frac{1}{14a} \sqrt{\frac{p_{\min}}{p_{\max}}} \frac{1}{\sqrt{p_{\min}}} \|\tilde{\Delta}\|_{2,1} \\
 &\leq \frac{1}{14a} \sqrt{\frac{1}{p_{\max}}} \|\Delta\|_{2,1}.
 \end{aligned}$$

The (2, 1)-norm term is now bounded using (16). Putting everything together we get

$$\begin{aligned}
 \|\hat{\beta}_i - \beta_i^*\|_{2,\infty} &\leq \|\widehat{\Sigma}(\hat{\beta}_i - \beta_i^*)\|_{2,\infty} + \|(\widehat{\Sigma} - I_{pd \times pd})(\hat{\beta}_i - \beta_i^*)\|_{2,\infty} \\
 &\leq \lambda\sqrt{p_{\max}} + \frac{2}{14a} \sqrt{\frac{1}{p_{\max}}} \left(\frac{24\lambda p^{\pi(i)}}{\kappa^2} \right) \\
 &\leq \left(1 + \frac{24}{7\kappa^2 a} \right) \lambda\sqrt{p_{\max}}.
 \end{aligned}$$

To satisfy both assumptions (A.1, 4.1), we need to set $a\kappa^2 = (a-1)$ as per Lemma A.4.

Finally, to prove the final claim, note that (19) combined with our sparsity assumption on the true parameters implies that for all $j' \neq \pi(i)$ it must be that $\|\hat{\beta}_i^{j'}\| = \|\hat{\beta}_i^{j'} - (\beta_i^*)^{j'}\| < c\lambda\sqrt{p_{\max}}$. We will show that for $\pi(i)$ it must be that $\|\hat{\beta}_i^{\pi(i)}\| > c\lambda\sqrt{p_{\max}}$. Hence, the estimator gets the correct index with high probability. Indeed, if $\|(\beta_i^*)^{\pi(i)}\| > 2c\lambda\sqrt{p_{\max}}$ we get

$$\begin{aligned}
 \|\hat{\beta}_i^{\pi(i)}\| &= \|(\beta_i^*)^{\pi(i)} - ((\beta_i^*)^{\pi(i)} - \hat{\beta}_i^{\pi(i)})\| \\
 &\geq \left| \|(\beta_i^*)^{\pi(i)}\| - \|((\beta_i^*)^{\pi(i)} - \hat{\beta}_i^{\pi(i)})\| \right| \\
 &\geq 2c\lambda\sqrt{p_{\max}} - c\lambda\sqrt{p_{\max}} \\
 &= c\lambda\sqrt{p_{\max}}.
 \end{aligned}$$

■

Let us restate the specific version of Theorem 4.2 again for clarity. This theorem is now a corollary of Theorem A.5.

Theorem 4.2. *Suppose the data have been pre-processed to satisfy (5) and let Assumption (4.1) hold. Take $\lambda \geq 4\lambda_0$, where*

$$\lambda_0 = \frac{2\sigma}{\sqrt{n}} \sqrt{1 + \sqrt{\frac{8 \log(d/\delta)}{p}} + \frac{8 \log(d/\delta)}{p}},$$

and set $c = \left(1 + \frac{24}{7(a-1)}\right)$. Then, for any $\delta \in (0, 1)$, any solution $\hat{\beta}_i$ of the Group Lasso objective (3) satisfies

$$\|\hat{\beta}_i - \beta_i^*\|_{2,\infty} \leq c\lambda\sqrt{p} \quad (6)$$

with probability at least $1 - \frac{\delta}{d}$.

If, in addition, $\|(\beta_i^*)^{\pi(i)}\| > 2c\lambda\sqrt{p}$, then (6) implies that

$$\hat{J}_i = \arg \max_{j=1,\dots,d} \|\hat{\beta}_i^j\|$$

estimates $\pi(i)$ correctly.

Proof The result follows from Theorem A.5, where in this case $k = d$, and $p^j = p$ for all $j = 1, \dots, d$. ■

Corollary A.6. *Assume the same setting as Theorem 4.2 such that for each $i = 1, \dots, d$, $\|(\beta_i^*)^{\pi(i)}\| > 2c\lambda\sqrt{p}$ and consider the estimator $\hat{\pi}$ as defined in (7). Then $\hat{\pi} = \pi$ with probability at least $1 - \delta$.*

Proof Consider the following estimators

$$\begin{aligned} \hat{\beta}_i &= \arg \min_{\beta \in \mathbb{R}^{dp}} \|\mathbf{C}_i - \Phi\beta\|^2 + \lambda\sqrt{p}\|\beta\|_{2,1}, \\ \hat{J}_i &= \arg \max_{j=1,\dots,d} \|\hat{\beta}_i^j\|, \\ \tilde{\pi} : [d] &\rightarrow [d], i \mapsto \hat{J}_i. \end{aligned}$$

We will first show that $\tilde{\pi}$ estimates π with probability at least $1 - \delta$. Afterwards, we will show that the event on which $\tilde{\pi}$ is correct, is contained in the event that $\hat{\pi}$ estimates π correctly, implying a lower bound on the requested probability.

We apply a union bound

$$\begin{aligned} \mathbb{P}(\tilde{\pi} = \pi) &= \mathbb{P}(\forall i = 1, \dots, d \mid \hat{J}_i = \pi(i)) \\ &= 1 - \mathbb{P}(\exists i = 1, \dots, d \mid \hat{J}_i \neq \pi(i)) \\ &> 1 - \sum_{i=1}^d \frac{\delta}{d} \\ &= 1 - \delta. \end{aligned}$$

We proceed to the second step. If $\tilde{\pi}$ estimates π correctly, then $\tilde{\pi}$ is already a valid permutation and $\tilde{\pi} = \hat{\pi}$. Indeed, if $\tilde{\pi}$ is correct then that means that $\|\hat{\beta}_i^{\tilde{\pi}(i)}\| = \|\hat{\beta}_i^{\pi(i)}\|$ is the maximum norm for each i . Coincidentally, by π being a correct permutation, $\tilde{\pi}$ describes a correct matching with largest values, which means that $\tilde{\pi}(i) = \hat{\pi}(i)$ for each $i = 1, \dots, d$ and

$$\mathbb{P}(\hat{\pi} = \pi) \geq \mathbb{P}(\tilde{\pi} = \pi) \geq 1 - \delta. \quad \blacksquare$$

B Proofs of Kernelized Permutation Estimator

We will make one adjustment to the Group Lasso regularization in the optimization problem in (8), which is that we square the regularization term. This form is theoretically more appealing, but is still equivalent to the standard formulation. As Bach (2008) argues, the two versions of the optimization problem will have the same set of solutions when varying the regularization parameters. For $\mu > 0$, the objective is given by

$$\inf_{\beta^1, \dots, \beta^d} \frac{1}{n} \|\mathbf{C}_i - \beta(\mathbf{M})\|^2 + \mu \left(\sum_{j=1}^d \|\beta^j\|_{\mathcal{H}_j} \right)^2. \quad (20)$$

Let $\widehat{\beta}_i^1, \dots, \widehat{\beta}_i^d$ be the solutions of the above optimization problem. The translation between regularization parameters that give the same solutions for (8) and (20) is given by $\lambda = \mu \left(\sum_{j=1}^d \|\widehat{\beta}_i^j\|_{\mathcal{H}_j} \right)$.

B.1 Representer Theorem

The squared version of the optimization problem allows us to prove the Representer theorem from the main text:

Theorem 5.1. *Let $\varphi_1, \dots, \varphi_d$ be the feature maps associated with $\mathcal{H}_1, \dots, \mathcal{H}_d$. Then there exist $\widehat{c}_i^1, \dots, \widehat{c}_i^d \in \mathbb{R}^n$ such that the optimization problem in (8) has solution $\widehat{\beta}_i$ with each $\widehat{\beta}_i^j$ of the form*

$$\widehat{\beta}_i^j = \sum_{\ell=1}^n \varphi_j(M_j^{(\ell)})(\widehat{c}_i^j)_\ell.$$

Proof First we state the following result about a variational equality for positive numbers

$$\left(\sum_{j=1}^d \|\beta^j\| \right)^2 = \inf_{\eta \in \Delta_d} \sum_{j=1}^d \frac{\|\beta^j\|^2}{\eta^j}. \quad (21)$$

A proof of this statement can be found in section 1.5 of (Bach et al., 2012). Using (21) and switching to the squared version of (8) we rewrite (20) as

$$\begin{aligned} & \inf_{\beta_1, \dots, \beta_d} \frac{1}{n} \|\mathbf{C}_i - \beta(\mathbf{M})\|^2 + \mu \left(\sum_{j=1}^d \|\beta^j\|_{\mathcal{H}_j} \right)^2 \\ &= \inf_{\eta \in \Delta_d} \inf_{\beta_1, \dots, \beta_d} \frac{1}{n} \|\mathbf{C}_i - \beta(\mathbf{M})\|^2 + \mu \sum_{j=1}^d \frac{\|\beta^j\|_{\mathcal{H}_j}^2}{\eta_j} \\ &= (\text{OPT}_1). \end{aligned}$$

We can rewrite this expression further, using the reproducing property of the RKHSs \mathcal{H}_j , which gives $\beta^j(M_j) = \langle \beta^j, \varphi_j(M_j) \rangle$. Furthermore, defining $\widetilde{\beta}^j = \frac{\beta^j}{\sqrt{\eta_j}}$ and $\widetilde{\varphi}_j = \sqrt{\eta_j} \varphi_j$ we rewrite

$$\begin{aligned}
 (\text{OPT}_1) &= \inf_{\eta \in \Delta_d} \inf_{\beta_1, \dots, \beta_d} \frac{1}{n} \sum_{\ell=1}^n \left(C_i^\ell - \sum_{j=1}^d \langle \beta^j, \varphi_j(M_i^{(\ell)}) \rangle \right)^2 + \mu \sum_{j=1}^d \frac{\|\beta^j\|_{\mathcal{H}_j}^2}{\eta_j} \\
 &= \inf_{\eta \in \Delta_d} \inf_{\widetilde{\beta}_1, \dots, \widetilde{\beta}_d} \frac{1}{n} \sum_{\ell=1}^n \left(C_i^{(\ell)} - \sum_{j=1}^d \langle \sqrt{\eta_j} \widetilde{\beta}^j, \varphi_j(M_j^{(\ell)}) \rangle \right)^2 + \mu \sum_{j=1}^d \|\widetilde{\beta}^j\|_{\mathcal{H}_j}^2 \\
 &= \inf_{\eta \in \Delta_d} \inf_{\widetilde{\beta}_1, \dots, \widetilde{\beta}_d} \frac{1}{n} \sum_{i=1}^n \left(C_i^{(\ell)} - \sum_{j=1}^d \langle \widetilde{\beta}^j, \widetilde{\varphi}_j(M_j^{(\ell)}) \rangle \right)^2 + \mu \sum_{j=1}^d \|\widetilde{\beta}^j\|_{\mathcal{H}_j}^2 \\
 &= (\text{OPT}_2).
 \end{aligned}$$

This final expression should be recognized as the feature representation of the Representer theorem (Schölkopf et al., 2001) applied to the kernel described by

$$\begin{aligned}
 \kappa(\eta)(M, M') &= \sum_{j=1}^d \langle \widetilde{\varphi}_j(M_j), \widetilde{\varphi}_j(M'_j) \rangle \\
 &= \sum_{j=1}^d \eta_j \langle \varphi_j(M_j), \varphi_j(M'_j) \rangle \\
 &= \sum_{j=1}^d \eta_j \kappa_j(M_j, M'_j).
 \end{aligned}$$

The Representer theorem then gives us that the solution of the inner optimization problem in (OPT₂) can be described by

$$\widetilde{\beta}^j = \sum_{\ell=1}^n \widetilde{\varphi}_j(M_j^{(\ell)})(c)_\ell \iff \frac{\beta^j}{\sqrt{\eta_j}} = \sqrt{\eta_j} \sum_{\ell=1}^n \varphi_j(M_j^{(\ell)})(c)_\ell \iff \beta^j = \sum_{\ell=1}^n \varphi_j(M_j^{(\ell)}) \eta_j (c)_\ell$$

with $c \in \mathbb{R}^n$ and $\eta \in \Delta_d$. Alternatively interpreted this says that there exist $c^1, \dots, c^d \in \mathbb{R}^n$ such that $\beta^j = \sum_{\ell=1}^n \varphi_j(M_j^{(\ell)})(c^j)_\ell$. We invoke again the equivalence between the squared and un-squared versions of the optimization problem using the translation of regularization parameters $\lambda = \mu \left(\sum_{j=1}^d \|\widehat{\beta}_i^j\|_{\mathcal{K}_j} \right)$ and conclude that the solutions of (8) are of the same form. ■

To get the finite-dimensional optimization problem as stated in (9) we substitute the correct forms of $\widehat{\beta}_i^j$ back into the original optimization problem. Define the Gramm matrices $(K_j)_{\ell k} = \kappa_j(M_j^{(\ell)}, M_j^{(k)}) = \langle \varphi_j(M_j^{(\ell)}), \varphi_j(M_j^{(k)}) \rangle$ and observe

$$\begin{aligned}
 &\inf_{\beta_1, \dots, \beta_d} \frac{1}{n} \sum_{\ell=1}^n \left(C_i^{(\ell)} - \sum_{j=1}^d \langle \beta^j, \varphi_j(M_j^{(\ell)}) \rangle \right)^2 + \lambda \sum_{j=1}^d \|\beta^j\|_{\mathcal{H}_j} \\
 &= \inf_{c^1, \dots, c^d \in \mathbb{R}^n} \frac{1}{n} \sum_{\ell=1}^n \left(C_i^{(\ell)} - \sum_{j=1}^d (K_j c^j)_i \right)^2 + \lambda \sum_{j=1}^d \sqrt{(c^j)^\top K_j c^j} \\
 &= \inf_{c^1, \dots, c^d \in \mathbb{R}^n} \frac{1}{n} \|\mathbf{C}_i - \sum_{j=1}^d K_j c^j\|^2 + \lambda \sum_{j=1}^d \|c^j\|_{K_j}.
 \end{aligned}$$

B.2 Estimator consistency

As stated in the main text, the assumptions in Theorem 5.2 are explained in this section. The assumptions stated in (A–D) ensure that the RKHSs that we work with are nice enough and that the function we want to estimate is not too miss specified. For a more complete discussion on the assumptions, we refer to Bach (2008). To remind ourselves, we are given d random variables $M = (M_1, \dots, M_d)$, where each random variable lives in \mathcal{Z}_j , and d RKHSs $\mathcal{H}_1, \dots, \mathcal{H}_d$ associated with d kernels $\kappa_1, \dots, \kappa_j$. The cross-covariance operator, Σ_{ij} for \mathcal{H}_j to \mathcal{H}_i is defined such that for all $(\beta^i, \beta^j) \in \mathcal{H}_i \times \mathcal{H}_j$,

$$\langle \beta^j, \Sigma_{ij} \beta^i \rangle = \mathbb{E}[\beta^i(M_i) \beta^j(M_j)] - \mathbb{E}[\beta^i(M_i)] \mathbb{E}[\beta^j(M_j)]. \quad (22)$$

The bounded correlation operators ρ_{ij} are defined through the decomposition $\Sigma_{ij} = \Sigma_{ii}^{1/2} \rho_{ij} \Sigma_{jj}^{1/2}$ (Baker, 1973).

- (A) For each $j = 1, \dots, d$, the Hilbert space \mathcal{H}_j is a separable reproducing kernel Hilbert space associated with kernel κ_j and the random variables $\kappa_j(\cdot, M_j)$ are not constant and have finite fourth-order moments.
- (B) For all $i, j = 1, \dots, d$, the cross correlation operators are compact ρ_{ij} and the joint correlation operator is invertible.
- (C) For each $i = 1, \dots, d$, there exist functions $\beta_i^{*1}, \dots, \beta_i^{*d} \in \mathcal{H}_1, \dots, \mathcal{H}_d$, $b_i \in \mathbb{R}$ and a function f_i of M such that

$$C_i = \sum_{j=1}^d \beta_i^{*j}(M_j) + b_i + f_i(M) + \varepsilon_i,$$

where $\mathbb{E}[\varepsilon_i | M] = 0$ and $\sigma_{\min}^2 < \mathbb{E}[\varepsilon_i^2 | M] < \sigma_{\max}^2$ with $\mathbb{E}[f_i(M)^2] < \infty$, $\mathbb{E}[f_i(M)] = 0$ and $\mathbb{E}[f_i(M) \beta_i^{*j}(M_j)] = 0$ for all $j = 1 \dots, d$. We define $\pi(i)$ to be the one index for which $\beta_i^{*\pi(i)} \neq 0$.

- (D) For all $i, j = 1, \dots, d$, there exists $g_i^j \in \mathcal{H}_j$ such that $\beta_i^{*j} = \Sigma_{jj}^{1/2} g_i^j$.

For each function, $\beta_i^{*\pi(i)}$, that is non-zero we will require the following condition

$$\max_{j \neq \pi(i)} \left\| \Sigma_{jj}^{1/2} \rho_{i\pi(i)} \rho_{\pi(i)\pi(i)}^{-1} D g_{\pi(i)} \right\|_{\mathcal{H}_i} < 1, \quad (23)$$

Where D is a block diagonal operator where each block consists of the operators $\frac{1}{\|\beta_i^{*j}\|_{\mathcal{H}_j}} I_{\mathcal{H}_j}$. Condition (B) can be seen as an analogue to the correlation assumption in Assumptions 4.1 and A.3, as it ensures that the variables are not too dependent.

Before we prove Theorem 5.2, we will first prove that each individual index $\pi(i)$ can be estimated consistently. This follows from an asymptotic result by Bach (2008).

Theorem 5.2. *Assume (A–D) in Appendix B.2. Then, for any sequence of regularization parameters λ_n such that $\lambda_n \rightarrow 0$ and $\sqrt{n} \lambda_n \rightarrow +\infty$ when $n \rightarrow \infty$, the estimated permutation $\hat{\pi}$ converges in probability to π .*

Proof To prove this result we first define the estimator of each individual index $\pi(i)$ as

$$\hat{J}_i = \arg \max_{j=1, \dots, d} \|\hat{\beta}_i^j\|_{\mathcal{H}_j}. \quad (24)$$

Theorem 11 in (Bach, 2008) gives consistency for the estimated parameters $\hat{\beta}_i^j$ and estimated index \hat{J}_i . However, his result is stated for the squared version of the Group Lasso and has as assumption that the μ_n regularization parameters have the property that $\mu_n \rightarrow \infty$ and $\sqrt{n} \mu_n \rightarrow +\infty$ as the number of data points $n \rightarrow \infty$. The translation factor between regularization parameters $\lambda_n = \mu_n (\sum_{j=1}^d \|\hat{\beta}_i^j\|_{\mathcal{H}_j})$ convergence to a

constant in probability, by the consistency of the estimated parameters. This shows that the scalings for λ_n and μ_n are the same asymptotically. We conclude that \widehat{J}_i estimates $\pi(i)$ with probability tending to 1.

Remember that the norms of $\widehat{\beta}_i^j$ and \widehat{c}_i^j are the same through $\|\widehat{\beta}_i^j\|_{\mathcal{H}_j} = \|\widehat{c}_i^j\|_{K_j}$. This means that we have consistency for estimators of $\pi(i)$ that are based on $\|\widehat{c}_i^j\|_{K_j}$ as well. For each $i = 1, \dots, d$ we can repeat the above argumentation to get consistency for each \widehat{J}_i separately. To combine the conclusions, we apply the same argument as in the finite dimensional case and a union bound that finishes our proof,

$$\begin{aligned} \mathbb{P}(\widehat{\pi} = \pi) &\geq 1 - \mathbb{P}(\exists i = 1, \dots, d \mid \widehat{J}_i \neq \pi(i)) \\ &\geq 1 - \sum_{i=1}^d \mathbb{P}(\widehat{J}_i \neq \pi(i)) \rightarrow 1. \end{aligned}$$

■

B.3 Implementation

Lemma B.1. For each $j = 1, \dots, d$ let L_j be the Cholesky decomposition of the Gram matrix K_j and let $\widehat{\gamma}_i^1, \dots, \widehat{\gamma}_i^d$ be minimizers of

$$\min_{\gamma^1, \dots, \gamma^d \in \mathbb{R}^n} \frac{1}{n} \|\mathbf{C}_i - \sum_{j=1}^d L_j \gamma^j\|^2 + \lambda \|\gamma^j\|_{2,1}. \quad (10)$$

Then $\widehat{c}_i^j = (L_j^\top)^{-1} \widehat{\gamma}_i^j$.

Proof Applying the Cholesky decomposition $K_j = L_j L_j^\top$ for each $j = 1, \dots, d$ and substituting this into (10) gives

$$\begin{aligned} \inf_{c^1, \dots, c^d \in \mathbb{R}^n} \frac{1}{n} \|\mathbf{C}_i - \sum_{j=1}^d K_j c^j\|^2 + \lambda \sum_{j=1}^d \|c^j\|_{K_j} &= \inf_{c^1, \dots, c^d \in \mathbb{R}^n} \frac{1}{n} \|\mathbf{C}_i - \sum_{j=1}^d L_j L_j^\top c^j\|^2 + \lambda \sum_{j=1}^d \|L_j^\top c^j\| \\ &= \inf_{\gamma^1, \dots, \gamma^d \in \mathbb{R}^n} \frac{1}{n} \|\mathbf{C}_i - \sum_{j=1}^d L_j \gamma^j\|^2 + \lambda \sum_{j=1}^d \|\gamma^j\|. \end{aligned}$$

■

The number of parameters now scales with the number of data samples. Computationally, this quickly becomes unwieldy. We apply a Nyström style approximation by sub-sampling $m \ll n$ columns of each K_j Gram matrix and using those to approximate the full Gram matrix (Williams and Seeger, 2000).

C Probability Results

Lemma C.1. For $j = 1, \dots, d$ and $\sigma^2 > 0$ let $\frac{\chi_j^2}{\sigma^2}$ be independent chi-square distributed random variables with p^j degrees of freedom for $j = 1, \dots, d$. Then, with $\delta \in (0, 1)$ and for

$$\lambda_0 = \frac{2\sigma}{\sqrt{n}} \sqrt{1 + \sqrt{\frac{4 \log(d/\delta)}{p_{\min}} + \frac{4 \log(d/\delta)}{p_{\min}}}},$$

we have

$$\mathbb{P} \left(\max_{1 \leq j \leq d} \frac{\chi_j}{\sqrt{np^j}} \leq \frac{\lambda_0}{2} \right) \geq 1 - \delta.$$

Proof This is Lemma 8.1 in (Bühlmann and Van De Geer, 2011) and substituting $x = \log(1/\delta)$. ■

The previous lemma is the general version of a concentration inequality that is need in the proof of Theorem A.5. The concentration inequality that we want to use is the following.

Lemma C.2. *Let $\sigma^2 > 0$ and assume that $\varepsilon^{(1)}, \dots, \varepsilon^{(n)}$ are independently $\mathcal{N}(0, \sigma^2)$ distributed, Φ as in Appendix A, and with $\delta \in (0, 1)$ set $\lambda \geq 4\lambda_0$ for*

$$\lambda_0 = \frac{2\sigma}{\sqrt{n}} \sqrt{1 + \sqrt{\frac{4 \log(d/\delta)}{p_{\min}}} + \frac{4 \log(d/\delta)}{p_{\min}}}$$

Then, $\mathbb{P}(\mathcal{A}) \geq 1 - \delta$, where $\mathcal{A} = \bigcap_{j=1}^d \mathcal{A}_j$ with the events $\mathcal{A}_j = \{\frac{1}{n} \|(\Phi^\top \varepsilon)^j\| \leq \frac{\lambda \sqrt{p^j}}{2}\}$ for all $j = 1, \dots, d$ and $\varepsilon = [\varepsilon^{(1)}, \dots, \varepsilon^{(n)}]^\top$.

Proof By assumption, $I_{p^j \times p^j} = \widehat{\Sigma}_j = \frac{1}{n} (\Phi_j)^\top \Phi_j$ and the fact that $\varepsilon \sim \mathcal{N}(0, \sigma^2 I_{n \times n})$, we first see

$$\begin{aligned} \frac{1}{\sigma \sqrt{n}} (\Phi \varepsilon)^j &= \frac{1}{\sigma \sqrt{n}} \Phi_j^\top \varepsilon \\ &\sim \mathcal{N}(0, \frac{1}{n} \Phi_j^\top I_{n \times n} \Phi_j) \\ &\sim \mathcal{N}(0, I_{p^j \times p^j}). \end{aligned}$$

This shows us that $\frac{1}{\sigma^2 n} \|(\Phi^\top \varepsilon)^j\|^2$ has a chi-squared distribution. We can now apply Lemma C.1 by noticing that it holds also holds for $\lambda \geq 4\lambda_0 \geq \lambda_0$ and that

$$\bigcap_{j=1}^d \mathcal{A}_j = \left\{ \max_{1 \leq j \leq d} \frac{1}{\sqrt{np^j}} \frac{1}{\sqrt{n}} \|(\Phi \varepsilon)^j\| \leq \frac{\lambda}{2} \right\}.$$

■

D Experiment Details

All the code to reproduce the experiments and figures in this paper is provided as a GitHub repository at <https://github.com/HiddeFok/sample-efficient-learning-of-concepts>. The synthetic experiments were performed on a single 32-core CPU node (AMD Rome 7H12) with 56GB of RAM. The DL experiments were performed on single 18-core GPU node (NVIDIA A100 GPU and Intel XEON CPU) with 120GB of RAM.

D.1 Toy Dataset Experiments

The synthetic experiments can be subdivided into 4 sets, based on which features mapping is used. These features mappings are linear features, spline features, random Fourier features and kernels. Here, we will describe how the data is generated and what the hyperparameters of the features and kernels were.

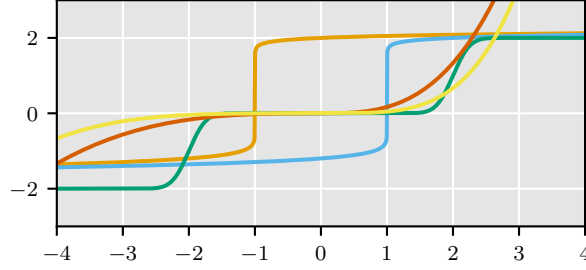


Figure 5: The diffeomorphisms used in the misspecified case

D.1.1 Data Generation

For the synthetic experiment we sample the $C \in \mathbb{R}^d$ variables from a $\mathcal{N}(0, (1 - \rho)I_{d \times d} + \rho\mathbb{1})$ distribution, where $\mathbb{1}$ denotes a matrix filled with only 1's. The $\rho \in (0, 1)$ parameter controls the amount of correlation between the variables. We sample n data points, on which we perform a 80/20 train/test data split. The test data is not needed to measure the performance of the permutation estimator, as we have access to the ground truth. We do use it to measure the risk or R^2 metric. There are 2 settings in which we generate the $M \in \mathbb{R}^d$ variables.

Wellspecified In the wellspecified setting we generate the M variables by applying a map consisting of the features and kernels used to estimate the permutation. This setting is a sanity check to see if our estimator works in a setting that satisfy all the required assumptions. For each dimension $j = 1, \dots, d$ a random weight vector $\beta_j^* \in \mathbb{R}^p$, such that $\|\beta_j^*\| \in [16\lambda_0, 32\lambda_0]$ uniformly. A permutation $\pi: \{1, \dots, d\} \rightarrow \{1, \dots, d\}$ is uniformly sampled from all possible permutations. Finally, with independent $\varepsilon_i \sim \mathcal{N}(0, \sigma^2)$ noise variables we get

$$C_i = \varphi(M_{\pi(i)})^\top \beta_{\pi(i)}^* + \varepsilon_i.$$

Misspecified In the misspecified setting we generate the M variables by first sampling d diffeomorphisms, $\{f_i: \mathbb{R} \rightarrow \mathbb{R}\}_{i=1}^d$ from a set of pre specified diffeomorphisms. These functions are plotted in Figure 5. Each function gets a random scaling w_i uniformly in $[-2, 2]$. Finally, we get

$$C_i = w_{\pi(i)} f_{\pi(i)}(M_{\pi(i)}) + \varepsilon_i.$$

For each of the experiments we save the MPE, R^2 score and execution time. To compare different settings of our estimator, we also save the MPE, R^2 and execution time of using only the purely linear version of our estimator on that particular data setting. We also save the MPE and execution times of using Pearson or Spearman correlations.

We vary the following parameters, the regularization parameter λ , the dimension d , the correlation ρ and the number of data points n . As stated before, in each experiment we look at the wellspecified and misspecified case.

- The regularization parameter varies in $\lambda \in \{0.001, 0.005, 0.01, 0.05, 0.1, 0.5, 1\}$. The other settings are set to $d \in \{20, 60, 100\}$, $\rho = 0$ and $n = 1250$.
- The dimension is varied in $d \in \{5, 30, 60, 80, 100\}$. The other settings are set to $\lambda \in \{0.001, 0.01, 0.1\}$, $\rho = 0$ and $n = 1250$.
- The correlation parameter varies in $\rho \in \{0, 0.2, 0.4, 0.6, 0.8, 0.95, 0.99\}$. The other settings are set to $\lambda \in \{0.001, 0.01, 0.1\}$, $d = 60$ and $n = 1250$.

- The dimension is varied in $n \in \{65, 125, 1250, 2500, 5000\}$. The other settings are set to $\lambda \in \{0.001, 0.01, 0.1\}$, $d = 60$ and $\rho = 0$.

D.1.2 Feature and Kernel setting

Linear features In the linear case no transformation is applied to the M variables.

Spline features In the spline features case we perform the regression using a spline basis transformation, either piecewise linear or cubic splines. We expect this method to work especially well, because the cubic splines form a dense subset in the space of twice differentiable functions, of which the diffeomorphisms are a subset. To calculate these features we use the `SplineTransformer` class of the `scikit-learn` package. The total number of feature parameters is calculated as $p = n_k + n_d - 1$, where n_k is the number of knots and n_d is the degree of each spline. In each of the toy dataset experiments the number of knots was $n_l \in \{4, 8\}$ and the degrees are $n_d \in \{1, 3\}$.

Random Fourier features For the random Fourier features we use a varying amount of random features. We sample random features that approximate the RBF kernel. To sample these features we use the `RBFsampler` class of the `scikit-learn` package. The total number of feature parameters in this case is number of random Fourier features. The number of features in the toy dataset experiments were $p \in \{2, 4, 6, 8\}$.

Kernels For the kernel experiments we perform the experiments for several kernels, the polynomial kernel, the RBF kernel, the Brownian kernel and a Sobolev kernel. These kernels are given by

$$\begin{aligned}\kappa_{\text{pol}}(x, y) &= (1 + \langle x, y \rangle)^3 \\ \kappa_{\text{RBF}}(x, y) &= e^{-(x-y)^2} \\ \kappa_{\text{Lap}}(x, y) &= e^{-|x-y|} \\ \kappa_{\text{cos}}(x, y) &= \cos(\langle x, y \rangle).\end{aligned}$$

D.2 Action/Temporal Dataset Experiments

The data generation settings, model architectures and training hyperparameters were taken from the original paper (Lachapelle et al., 2022). Their implementation can be found at https://github.com/slachapelle/disentanglement_via_mechanism_sparsity/tree/main.

D.2.1 Dataset Details

The dataset consists of temporal data sequences, $\{(X^t, z^t, a^t)\}_{t=1}^T$, where $X^t \in \mathbb{R}^{20}$ is the observed data, $a^t \in \mathbb{R}^{10}$ is an action, which is seen as an auxiliary variable in the ICA framework developed in (Khemakhem et al., 2020), and $z^t \in \mathbb{R}^{10}$ the latent causal variable. The ground truth mixing function f is a random neural network with three hidden layers of 20 units with Leaky-ReLU activations with negative slope of 0.2. The weight matrices are sampled independently according to $\mathcal{N}(0, 1)$ and the weight matrices are the orthogonalized to ensure inactivity of the mixing function. The observational noise ε in each dimension is sampled according $\mathcal{N}(0, 10^{-4})$ and is added to $f(z^t)$. The transitions from (z^{t-1}, a^{t-1}) to z^t is sampled according to $\mathcal{N}(\mu(z^{t-1}, a^{t-1}), 10^{-4}I_{10 \times 10})$. The mean function μ will be different between the Action Sparsity dataset and the Temporal Sparsity dataset.

Action Sparsity The sequences have length $T = 1$ and the mean function is given by

$$\mu(z^{t-1}, a^{t-1})_i := \sin\left(\frac{2+i}{\pi} a_i^{t-1} + (i-1)\right) + \sin\left(\frac{2+i}{\pi} a_{i-1}^{t-1} + (i-1)\right),$$

Table 2: Architecture details for the encoder and decoders used in the temporal and action sparsity dataset experiments.

	Layer	Hidden Size	Activation Function
Encoder	Linear	512	LeakyReLU(0.2)
	Linear	512	LeakyReLU(0.2)
	Linear	512	LeakyReLU(0.2)
	Linear	512	LeakyReLU(0.2)
	Linear	512	LeakyReLU(0.2)
	Linear	512	LeakyReLU(0.2)
	Linear	2 · 10	-
Decoder	Linear	512	LeakyReLU(0.2)
	Linear	512	LeakyReLU(0.2)
	Linear	512	LeakyReLU(0.2)
	Linear	512	LeakyReLU(0.2)
	Linear	512	LeakyReLU(0.2)
	Linear	512	LeakyReLU(0.2)
	Linear	20	-

where the index $i = -1$ is periodically identified with $i = 10$.

Temporal Sparsity The sequences have length $T = 2$ and the mean function is given by

$$\mu(z^{t-1}, a^{t-1})_i := z_i^{t-1} + 0.5 \sum_{j=1}^i \sin\left(\frac{2+j}{\pi} z_j^{t-1} + (i-1)\right).$$

In both datasets we sample 10^6 points and split the dat 80/20 for the train/test split.

D.2.2 Model Architectures

Table 3: The hyperparameters used for the training of the DMS-VAE, TCVAE and iVAE for the action and temporal sparsity datasets

Hyperparameter	Value
Batch Size	1024
Optimizer	Adam (Kingma and Ba, 2015) and Cooper (Gallego-Posada et al., 2021)
Learning rate	5e-4 (DMS-VAE), 1e-4 (iVAE), 1e-3 (TCVAE)
KL divergence factor β	1.0
Number of latents	20
Number of epochs	500
Gumbel Softmax temperature	1.0

In all experiments a minibatch of 1024 is used for the training. The same encoder and decoder is used for all models: A MLP with 6 layers of 512 units with LeakyReLU activations with negative slope 0.2. See Table 2 for a detailed description. The encoder $f_{\text{enc}}(x; \theta)$ outputs the mean and standard deviation of $q_{\theta}(z^t | x^t)$, which are the densities of normal distribution. The latent transition distribution $\hat{p}_{\lambda}(z_i^t | z^{<t}, a^{<t})$, where $z^{<t} = (z^{t'})_{t'=1}^{t-1}$ and $a^{<t} = (a^{t'})_{t'=1}^{t-1}$, is also also learned by a fully connected neural network. It’s parameters are λ and it outputs the variance of a $\mathcal{N}(0, \sigma^2)$ distribution. The decoder $f_{\text{dec}}(z; \psi)$ tries to reconstruct the original data from the learned encodings. The differences between the 3 methods comes from the loss function that is optimized. The common term in each of the optimizations is the Evidence Lower Bound (ELBO)



Figure 6: Examples of the 7 shapes in the Temporal Causal3DIdent dataset. From left to right: teapot, armadillo, bunny, cow, dragon, head and horse.

objective. This is given by

$$\text{ELBO}(\theta, \psi, \lambda) = \sum_{t=1}^T \mathbb{E}_{z^t \sim q_\theta(\cdot | x^t)} [\log p_\psi(x^t | z^t)] - \mathbb{E}_{z^{<t} \sim q_\theta(\cdot | x^{<t})} [\text{KL}(q_\theta(z^t | x^t) \| \hat{p}_\lambda(z^t | z^{<t}, a^{<t}))], \tag{25}$$

where $\text{KL}(\cdot \| \cdot)$ is the KL-divergence.

DMS-VAE A regularization term is added to the ELBO objective in (25). The regularization enforces sparsity to the learned graph describing the causal relations between the learned encodings and actions. The new objective is given by

$$\text{ELBO}(\theta, \psi, \lambda) + \alpha_z \|\hat{G}_z\|_0 + \alpha_a \|\hat{G}_a\|_0.$$

The variable \hat{G}_z is a learned matrix representing the relations between the latent variables between 2 time steps. The variable \hat{G}_a is a learned matrix representing the relations between the actions and the latent variables. The norm $\|\cdot\|_0$ counts the number of non-zero terms. This is a discrete objective and can be transformed into a continuous objective using the Gumbel-Softmax trick (Maddison et al., 2017; Jang et al., 2017).

Alternatively, The authors propose a constrained based optimization procedure on the ELBO, where the constrained is determined by the number of edges in the learned graph. For the constrained optimization method the authors provide a optimization schedule that performs this optimization procedure, which we use by setting the `--constraint_schedule` parameter. The other hyper parameters for the training procedure can be found in Table 3.

TCVAE The implementation of the original paper (Chen et al., 2018) was adapted by the authors of (Lachapelle et al., 2022), which we also use. The loss function consists of the same components as the ELBO in (25), but they decompose it into 3 terms and add a weight parameter to each of the terms. The hyper parameters for the training procedure can be found in Table 3.

iVAE The implementation of the original paper (Khemakhem et al., 2020) was adapted by the authors of (Lachapelle et al., 2022), which we use. The loss function here is very similar to the ELBO objective, but it adds one parameter β to the KL-term in the objective. The hyper parameters for the training procedure can be found in Table 3.

D.3 Temporal Causal3DIdent

The dataset, model architectures and training hyper parameters were taken from (Lippe et al., 2022). Their implementation can be found at <https://github.com/phlippe/CITRIS/tree/main>.

D.3.1 Dataset Details

The data comes from a setting which is referred to as Temporal Intervened Sequences. The assumption is that there are d causal variables (G_1, \dots, G_d) and a corresponding causal graph $\mathcal{G} = (V, E)$ where each node $i \in V$ represents a causal variable G_i . The variables can be real-valued or vector-valued, and each edge $(i, j) \in E$ represents a relation between G_i and G_j . Now, we assume there are T time steps and for every $t = 1, \dots, T$ the causal variables are generated through some process. So, we have a sequence $\{(G_1^t, \dots, G_d^t)\}_{t=1}^T$, where only the causal variables in $t - 1$ are the parents of the causal variables in time step t . Identifiability is achieved in this setting by assuming that we have access to d -dimensional binary vector at each time step $I^t \in \{0, 1\}^d$ that tells us which causal variables have been intervened on, but not with which value. The observations X^t at each time step are created through a mixing function and some noise $X^t = f(G_1^t, \dots, G_d^t, \varepsilon^t)$. The authors in Lippe et al. (2022) propose a framework, CITRIS, that is able to disentangle these causal variables into k encodings. The number of encodings is allowed to be bigger than d , but the model subdivides the encodings into d possibly uneven blocks that get mapped to the causal variables. They also altered the implementation of other methods, such as iVAE, to be able to work in their setting and show that CITRIS works the best.

The causal variables that are used in the data generating process are the following:

- The **object position** (`pos_o`) is modelled in 3 dimensions $(x, y, z) \in [-2, 2]^3$. The values are forced to be in this interval to ensure that the object does not disappear from the image, becomes too small or covers the whole image.
- The **object rotation** (`rot_o`) is modelled in 2 dimensions $(\alpha, \beta) \in [0, 2\pi)^2$. Distances for angles are calculated in a periodic fashion, ensuring that angles close to 0 and 2π are close together.
- The **spotlight rotation** (`rot_s`) is the positioning of the spotlight that shines on the object. The value range is $[0, 2\pi)$, where distances are again calculated in a periodic fashion.
- The **spotlight hue** (`hue_s`) is the color of the spotlight. The range of the value is $[0, 2\pi)$, where 0 corresponds to red.
- The **background hue** (`hue_b`) is the color of the background. The value range is $[0, 2\pi)$ with the 0 corresponding to red again.
- The **object hue** (`hue_o`) is the color of the object, with value range is $[0, 2\pi)$ and with again 0 representing red.

The authors in Lippe et al. (2022) generated the data using Blender, a setup inspired by von Kügelgen et al. (2021) and using code provided by Zimmermann et al. (2021). They generate the dataset by starting with an initial random set of causal variables. They then sample the causal variables in each subsequent time step by following a specific conditional distribution, which is given by the set of equations in (26).

$$\begin{aligned}
 f(a, b, c) &= \frac{a - b}{2} + c \\
 \text{pos}_x^{t+1} &= f(1.5 \cdot \sin(\text{rot}_\beta^t), \text{pos}_x^t, \varepsilon_x^t) \\
 \text{pos}_y^{t+1} &= f(1.5 \cdot \sin(\text{rot}_\alpha^t), \text{pos}_y^t, \varepsilon_y^t) \\
 \text{pos}_z^{t+1} &= f(1.5 \cdot \sin(\text{rot}_\alpha^t), \text{pos}_z^t, \varepsilon_z^t) \\
 \text{rot}_\alpha^{t+1} &= f(\text{hue}_b^t, \text{rot}_\alpha^t, \varepsilon_\alpha^t) \\
 \text{rot}_\beta^{t+1} &= f(\text{hue}_o^t, \text{rot}_\beta^t, \varepsilon_\beta^t) \\
 \text{rot}_s^{t+1} &= f(\text{atan2}(\text{pos}_x^t, \text{pos}_y^t), \text{rot}_s^t, \varepsilon_{rs}^t) \\
 \text{hue}_s^{t+1} &= f(2\pi - \text{hue}_b^t, \text{hue}_s^t, \varepsilon_{hs}^t) \\
 \text{hue}_b^{t+1} &= \text{hue}_b^t + \varepsilon_b^t \\
 \text{hue}_o^{t+1} &= f(g(i), \text{hue}_o^t, \varepsilon_{ho}^t)
 \end{aligned} \tag{26}$$

All the noise ε -variables are independently $\mathcal{N}(0, 10^{-2})$ distributed for the position and $\mathcal{N}(0, (0.15)^2)$ distributed for the angels. The g function in the final line maps the object shapes to specific values detailed in Table 4.

The object shape is changed in each time step with a probability of 0.05. If it is changed, a new shape is sampled uniformly over the 7 shapes.

They then sample for each time step the intervention targets $I_i^{t+1} \sim \text{Bernoulli}(0.1)$. If a causal variables is intervened on it is replaced with a random sample from $U(-2, 2)$ for continuous values or $U(0, 2\pi)$ for the angles. For the object shape a uniform distribution over the 7 shapes is used. They run this generation for 250,000 steps, which is the full dataset.

We use the already generated dataset downloaded from <https://zenodo.org/records/6637749#.YqcWCnVBxCA>.

D.3.2 Model Architectures

In both the CITRIS-VAE and iVAE models, the encoder and decoder architecture are set to be the same. The encoder is a convolutional neural network, which outputs two parameters per latent variable. These will be the mean and the log of the standard deviation for the normal distribution that models the latent variable. The decoder uses bilinear upsampling and residual blocks to reconstruct the image. The full architecture is described in Table 5. For these experiments, the ELBO is defined to be

$$\begin{aligned} \text{ELBO}(\theta, \varphi, \gamma) = & - \mathbb{E}_{z^{t+1} \sim q_\theta(\cdot | x^{t+1})} [\log p_\theta(x^{t+1} | z^{t+1})] \\ & + \mathbb{E}_{\substack{z^t \sim q_\theta(\cdot | x^t) \\ \pi \sim \text{GS}(\gamma)}} \left[\sum_{i=1}^d \text{KL}(q_\theta(z_{\pi(i)}^{t+1} | x^{t+1}) \parallel p_\varphi(z_{\pi(i)}^{t+1} | z^t, I_i^{t+1})) \right]. \end{aligned}$$

Here p_θ models the encoder, q_θ the decoder, $p_\varphi(z^{t+1} | z^t, I^{t+1})$ the transition prior and GS is the Gumbel-Softmax distribution of the causal variables between time steps given the intervention targets. Finally, π is the target assignment between learned encoding variables and the causal variables.

To train the CITRIS-VAE and the iVAE method, an autoencoder is pre-trained to map the high-dimensional images to lower-dimensional feature vectors, but without enforcing disentanglement. This is done separately from the main training procedure as Lippe et al. (2022) mention that this improves performance. During training a small bit of Gaussian noise is added to the encodings to prevent collaps of the encoding distribution. No prior is enforced for this encoder. This autoencoder will be have 2 ResidualBlocks instead of 1 per resolution in the decoder part. The training hyperparameters are described in Table 7. The autoencoder is trained using the MSE reconstruction loss.

Table 4: Output of the g function for each object shape

Object shape	Object hue goal
Teapot Size	0
Armadillo	$\frac{2\pi}{5}$
Hare	$\text{avg}(\text{hue}_{s^t}, \text{hue}_{b^t})$
Cow	$\frac{4\pi}{5}$
Dragon	$\pi + \text{avg}(\text{hue}_{s^t}, \text{hue}_{b^t})$
Head	$\frac{6\pi}{5}$
Horse	$\frac{8\pi}{5}$

The avg function is defined as

$$\text{avg}(\alpha, \beta) = \text{atan2} \left(\frac{\sin(\alpha) + \sin(\beta)}{2}, \frac{\cos(\alpha) + \cos(\beta)}{2} \right).$$

Table 5: Architecture details for the encoder and decoders used in the Temporal Causal3DIdent experiments.

	Layer	Feature Dimension (H × W × C)	Kernel	Stride	Activation Function
Encoder	Conv	32 × 32 × 64	3	2	BatchNorm+SiLU
	Conv	32 × 32 × 64	3	1	BatchNorm+SiLU
	Conv	16 × 16 × 64	3	2	BatchNorm+SiLU
	Conv	16 × 16 × 64	3	1	BatchNorm+SiLU
	Conv	8 × 8 × 64	3	2	BatchNorm+SiLU
	Conv	8 × 8 × 64	3	1	BatchNorm+SiLU
	Conv	4 × 4 × 64	3	2	BatchNorm+SiLU
	Conv	4 × 4 × 64	3	1	BatchNorm+SiLU
	Reshape	1 × 1 × 1024	-	-	-
	Linear	1 × 1 × 256	-	-	LayerNorm+SiLU
	Linear	1 × 1 × 2 · num_latents	-	-	-
Decoder	Linear	1 × 1 × 256	-	-	LayerNorm+SiLU
	Linear	1 × 1 × 1024	-	-	-
	Reshape	4 × 4 × 1024	-	-	-
	Upsample	8 × 8 × 64	-	-	-
	ResidualBlock	8 × 8 × 64	3	1	-
	Upsample	16 × 16 × 64	-	-	-
	ResidualBlock	16 × 16 × 64	3	1	-
	Upsample	32 × 32 × 64	-	-	-
	ResidualBlock	32 × 32 × 64	3	1	-
	Upsample	64 × 64 × 64	-	-	-
	ResidualBlock	64 × 64 × 64	3	1	-
	Pre-Activations	64 × 64 × 64	-	-	BatchNorm+SiLU
	Conv	64 × 64 × 64	1	1	BatchNorm+SiLU
	Conv	64 × 64 × 3	1	1	Tanh

CITRIS-VAE In the CITRIS model, an assignment $\pi: \{1, \dots, k\} \rightarrow \{1, \dots, d\}$ is learned between the learned encodings, and the true causal variables. This done by assuming that each $\pi(i)$ follows a Gumbel-Softmax distribution and we learn the continuous parameter that governs this distribution. During training an encoding-to-causal variable assignment is sampled, while during inference the argmax is used.

The transition prior p_φ is learned by an autoregressive model, which for each $z_{\pi(i)}^{t+1}$ takes z^t, I_i^{t+1} and z^{t+1} as inputs and outputs a Gaussian random variable. The autoregressive model follows a MADE architecture (Khajenezhad et al., 2021), with 16 neurons per layer for each encoding, and the input to these neurons are the features of all previous encodings. The prior is 2 layers deep, and uses the SiLU activation function.

Finally, a small network is trained to predict the intervention targets, given z^t and $z_{\pi(i)}^{t+1}$ for each $i = 1, \dots, k$.

iVAE To adept the iVAE model for this setting, the auxiliary variable u will be given by the previous observation x^t and intervention targets I^{t+1} . Another alteration that is made is that the prior with the iVAE model only conditions on (x^t, I^{t+1}) . The main difference between iVAE and the CITRIS-VAE is the structure of the prior $p(z^{t+1} | z^t, I^{t+1})$. Another difference is that no target assignment is learned during the training, but only after.

For the iVAE a 2-layer MLP with hidden dimensionality of 128 is used for the transition prior.

D.4 Performance metrics

To assess the performance of our estimator we record the MPE of the estimated permutation, together with the execution time. On top of that we record the R^2 -score. Some of the baselines are created by regression every input variable onto every output variable and using the individual R^2 -scores to extract a permutation. In those

Table 6: The hyperparameters used for the training of both the CITRIS-VAE and iVAE models.

Hyperparameter	Value
Batch Size	512
Optimizer	Adam (Kingma and Ba, 2015)
Learning rate	1e-3
Learning rate scheduler	Cosine Warmup (100 steps)
KL divergence factor β	1.0
KL divergence factor $\psi_0(\lambda)$	0.01
Number of latents	32
Number of epochs	600
Target classifier weight	2.0
Gumbe Softmax temperature	2.0

Table 7: The hyperparameters used for the training of autoencoder used by both the CITRIS-VAE and iVAE.

Hyperparameter	Value
Batch Size	512
Optimizer	Adam (Kingma and Ba, 2015)
Learning rate	1e-3
Learning rate scheduler	Cosine Warmup (100 steps)
Number of latents	32
Gaussian noise σ	0.05
Number of epochs	1000

cases the R^2 -scores that is documented here in the paper is the average of the R^2 -scores that are chosen to be matched. This is also referred to as the R^2 -score on the diagonal. This gives

$$R^2 = \frac{1}{d} \sum_{i=1}^d \left(1 - \frac{\|\mathbf{C}_i - \widehat{h}_{\widehat{\pi}(i)}(\mathbf{M}_{\widehat{\pi}(i)})\|^2}{\|\mathbf{C}_i - \overline{\mathbf{C}}_i\|^2} \right), \quad \overline{\mathbf{C}}_i = \frac{1}{n} \sum_{\ell=1}^d C_i^{(\ell)}.$$

Here, \widehat{h}_j is the estimated mapping and it is applied to the whole vector \mathbf{M}_j .

Estimator settings We use various settings of our estimator, to asses if there are particular advantages for certain versions. The versions that we used were

- **Linear**, no feature map is applied.
- **random Fourier Features**, we sample 8 random Fourier features from the RBF kernel.
- **Spline**, we calculate cubic spline features with 6 knots.
- **Laplacian**, we use the Laplacian kernel with $\min\{n, 20\}$ components.
- **Two stage** we apply a two stage approach, where we use 20% of the data to estimate the permutation using no additional features and then use the rest of the data to perform ridge regression with cubic spline features using 6 knots.

We define an array of regularization parameters and report the results of the best choice for each n . The parameters that were considered are $\lambda \in \{0.0001, 0.0005, 0.001, 0.005, 0.01, 0.05, 0.1, 0.2\}$.

Baselines We again calculate the permutations using the Pearson and Spearman correlations. For these experiments, we added another baseline, which is given by trained neural networks. Each neural network takes an individual encoding as input and tries to predict all the causal variables. The individual R^2 -scores are used to construct a matching again. This neural network is a 2-layer MLP with 128 hidden nodes in each layer and using the tanh as an activation function. The network is trained for a 100 epochs with Adam and a learning rate of 4e-3. We considered using 32 and 64 hidden nodes and saw that 128 performed the best.

In the Temporal Causal3DIdent dataset experiments, both VAE models learn groups of encoded variables that are matched with a causal variable. To use the Pearson and Spearman correlations in this case, we first sum the encodings in the groups and then calculate the correlation coefficients.

E Additional Results

Here, we show all the results obtained in the experiments with the toy dataset, action/temporal sparsity dataset and temporal Causal3DIdent dataset.

E.1 Toy Dataset

We provide plots for experiments performed with linear features, spline features, random Fourier features and kernels.

In each of the version of our estimator we see that the MPE scores are good. Especially in the misspecified setting. It is interesting to note that the estimator does not perform well in the well-specified case, when the regularization parameter is not tuned correctly. This can be explained by the non-invertability of the functions in this setting. This makes the identification of each matching more noisy and difficult, which can also be noted by the fact that the Pearson and Spearman correlation approaches are not able to find the correct permutation, while our is able to.

This also explains why the R^2 scores in the well-specified case are worse than the R^2 -scores. Another reason for that observation is that norms of the true parameters have to be quite large, to strictly adhere to the assumptions of our theoretical results. This increases the variability of the output data by a large margin and makes regression more difficult.

Finally, we can also see that our estimator does work well, even when the correlation is high, but the regularization parameter has to be tuned correctly. This does come at a cost of an increasing computation time.

E.2 Action/Temporal Sparsity Datasets and Temporal Causal3DIdent Dataset

Here, we report all results obtained in the action/temporal sparsity datasets and temporal Causal3DIdent dataset. The MPEs are reported in Table 8, the R^2 -scores in Table 9 and the execution times are plotted in Figure 16.

In terms of MPE, we see that a version of our estimator performs the best or as good as the best in each of the datasets in terms of the number of samples need to get the permutation correct. For the R^2 -scores we see that we perform well in some cases in the low data regime, but when using all the data available, the neural network often performs the best. This does come at a computational cost, where the neural network approach requires two to three orders of magnitude more computation time.

It is interesting to note that the estimator typically works better for the more advanced models developed. This can be explained by the fact that these models achieve a better disentanglement, which should make it easier to find the correct matching between the encodings and the causal variables.

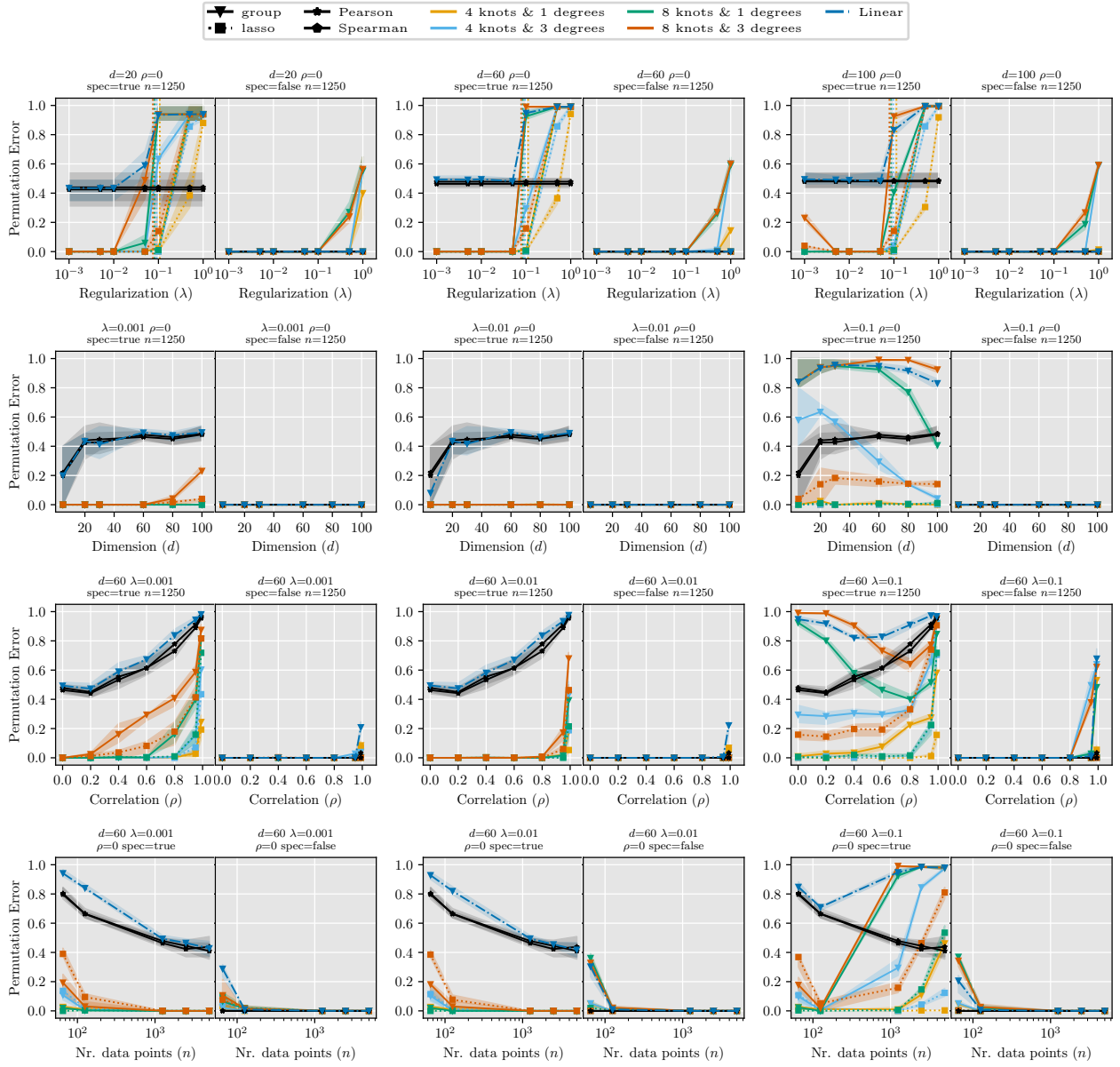


Figure 7: Permutation Error using Spline Features for all parameters

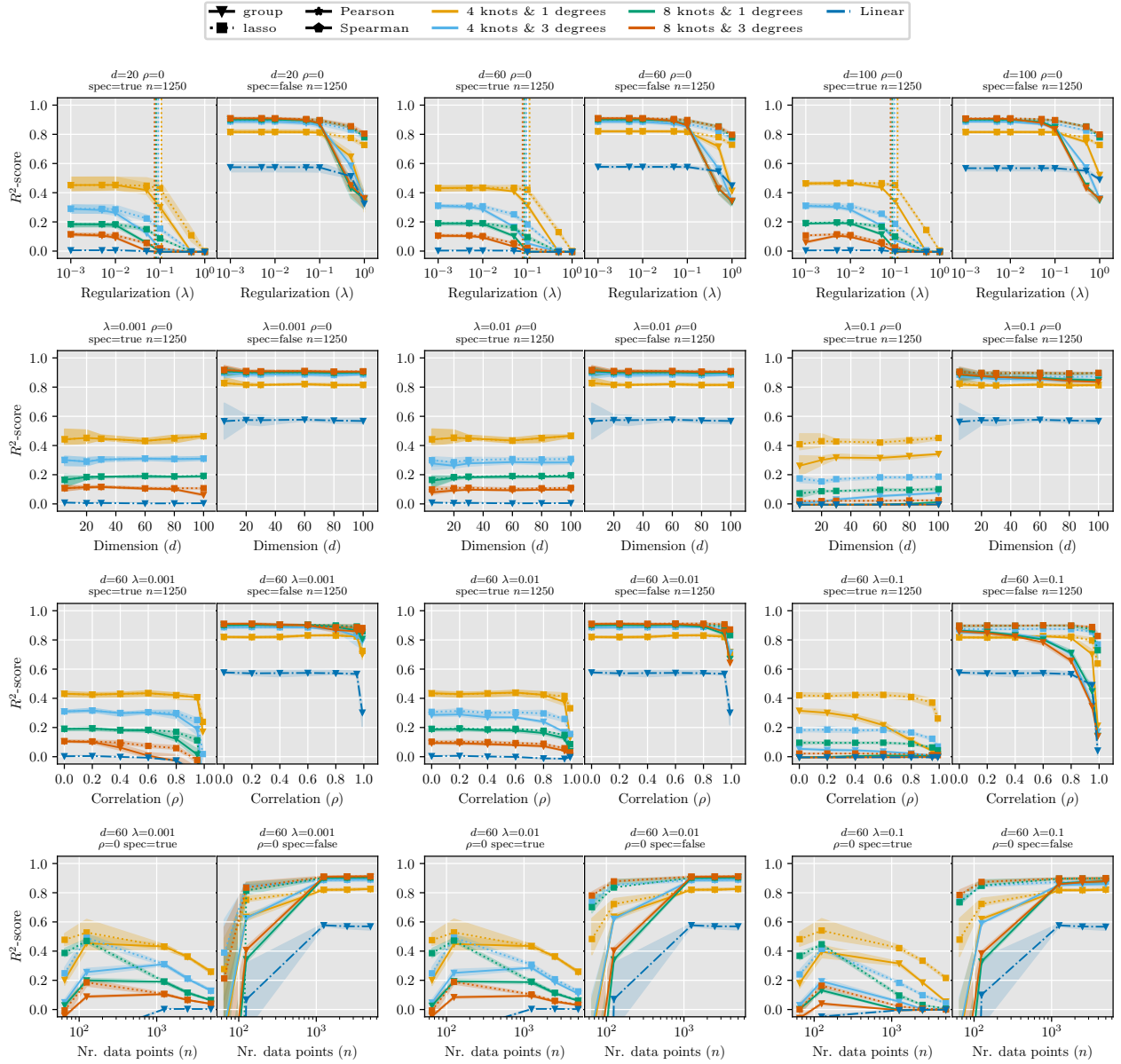


Figure 8: R^2 -score on the diagonal using Spline Features for all parameters

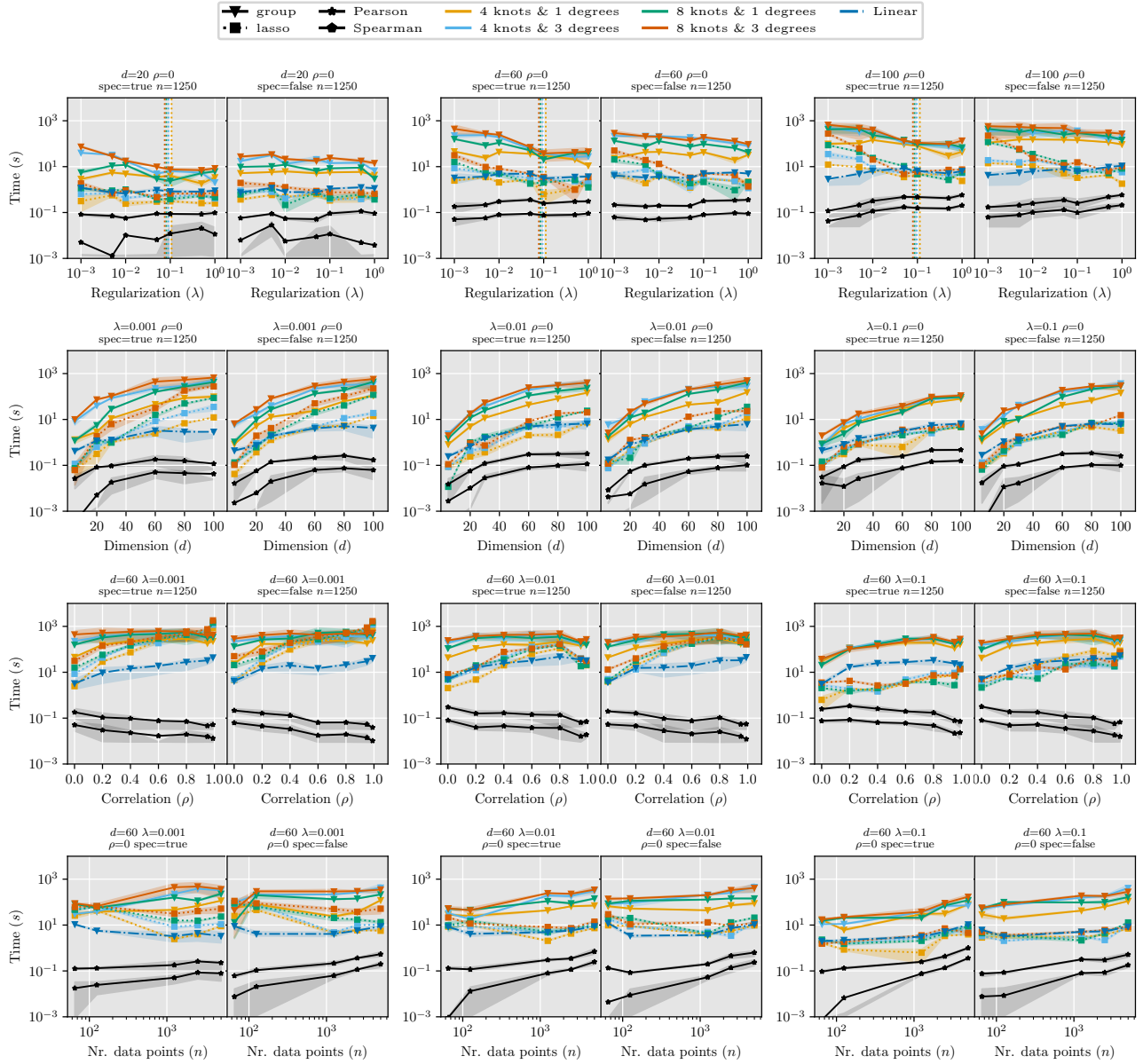


Figure 9: Execution times using Spline Features for all parameters

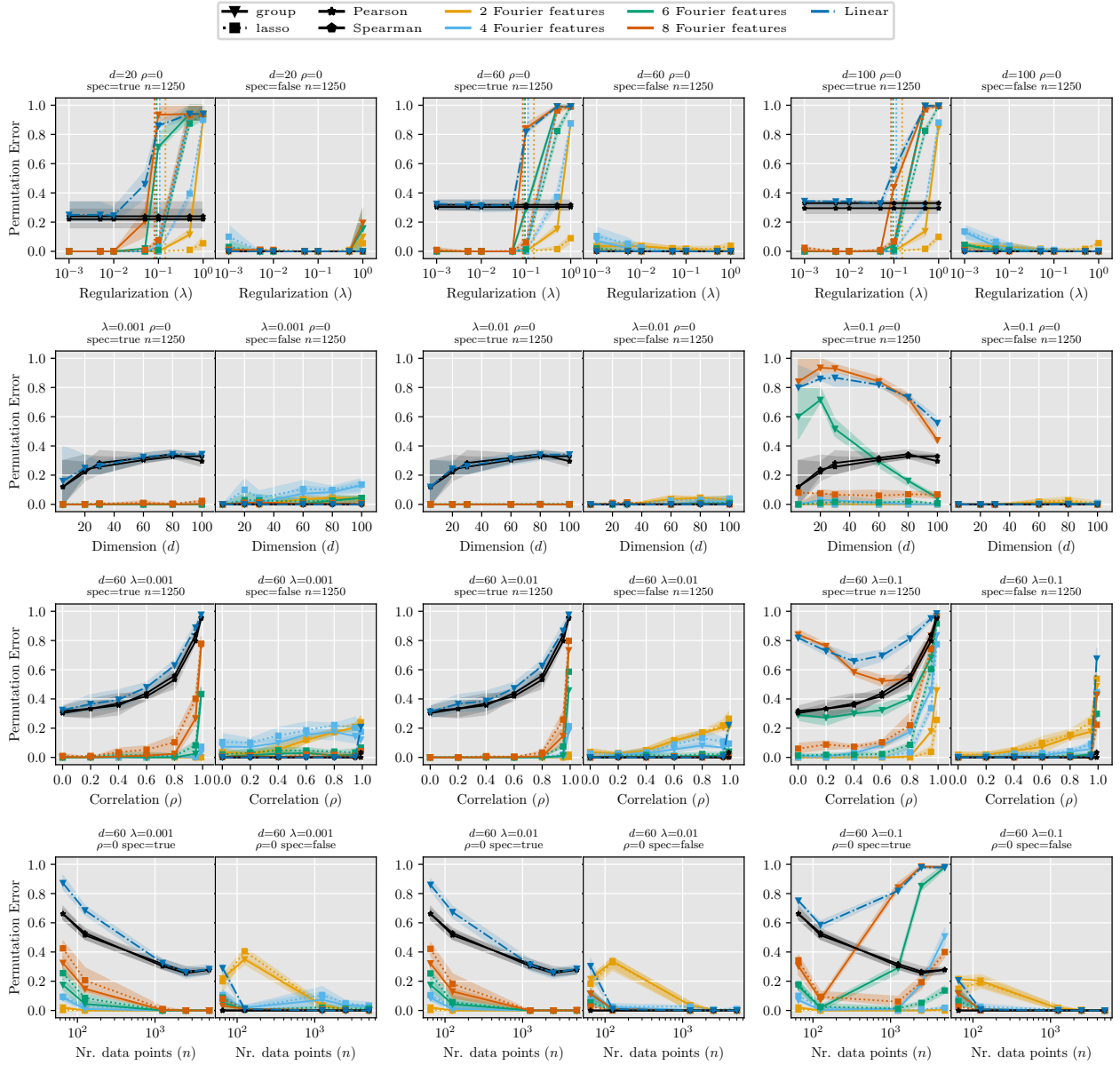


Figure 10: Permutation Errors using Random Fourier Features

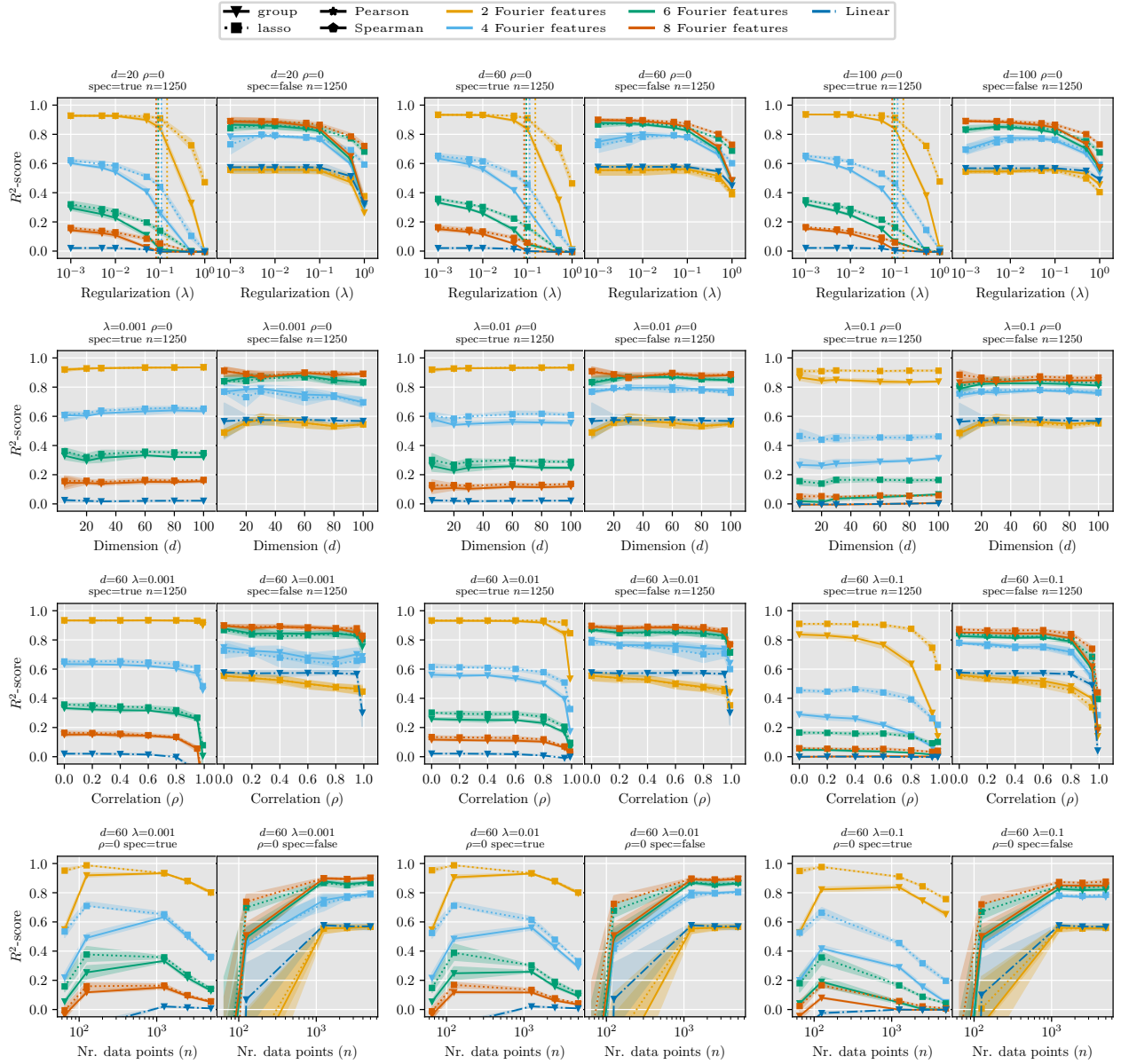


Figure 11: R^2 -score on the diagonal using Random Fourier Features

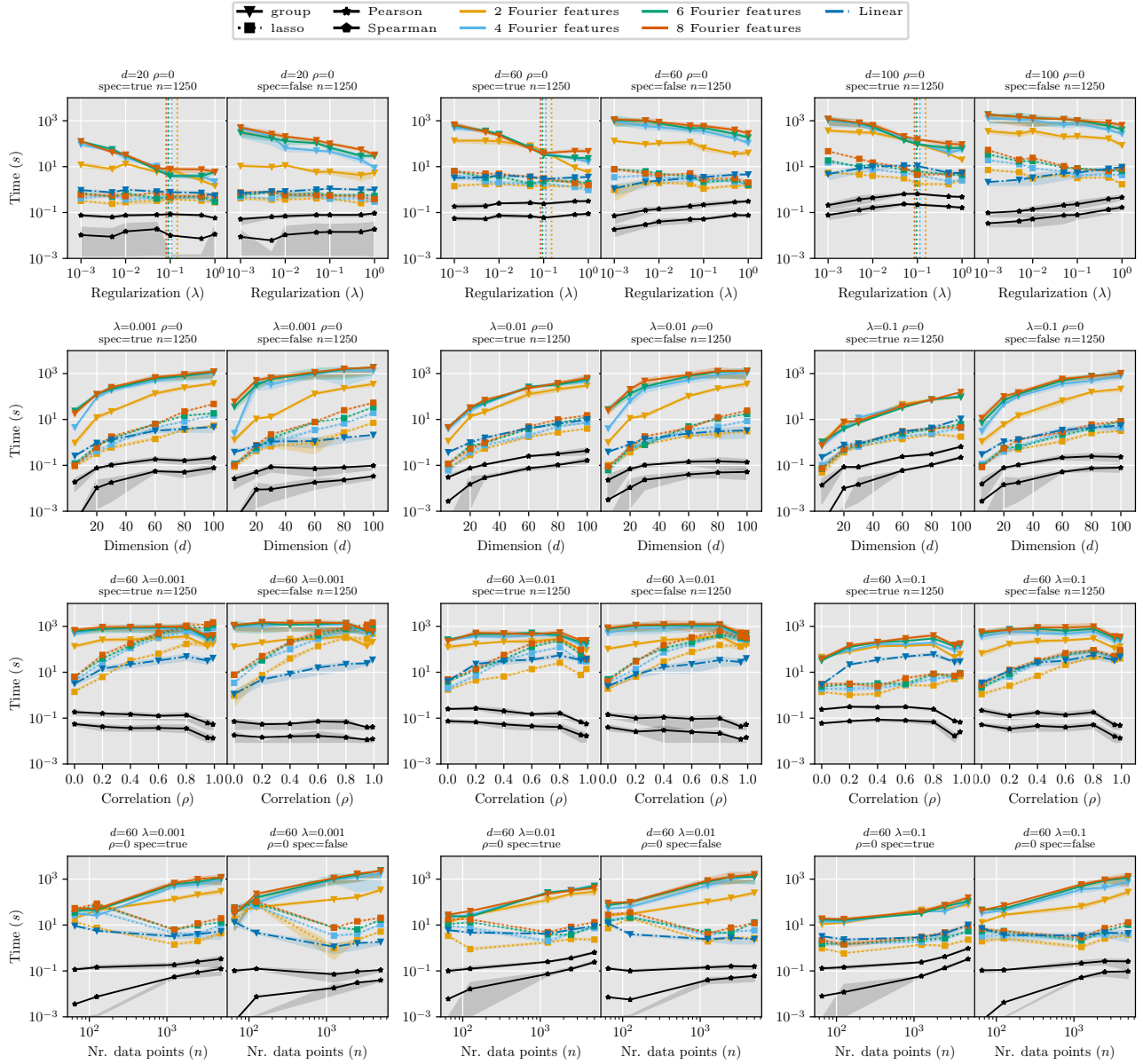


Figure 12: Execution times using Random Fourier Features

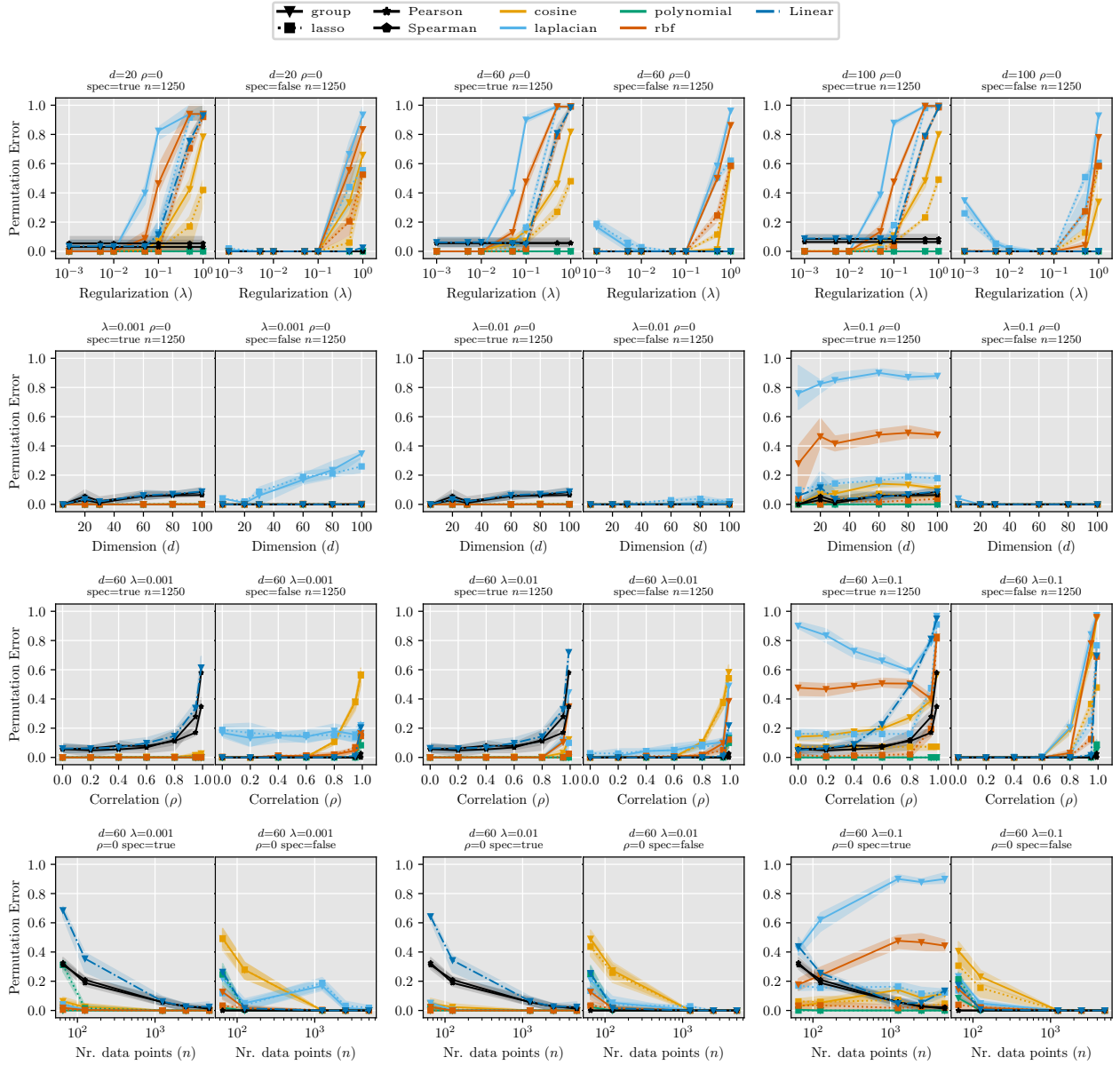


Figure 13: Permutation Errors using Kernels

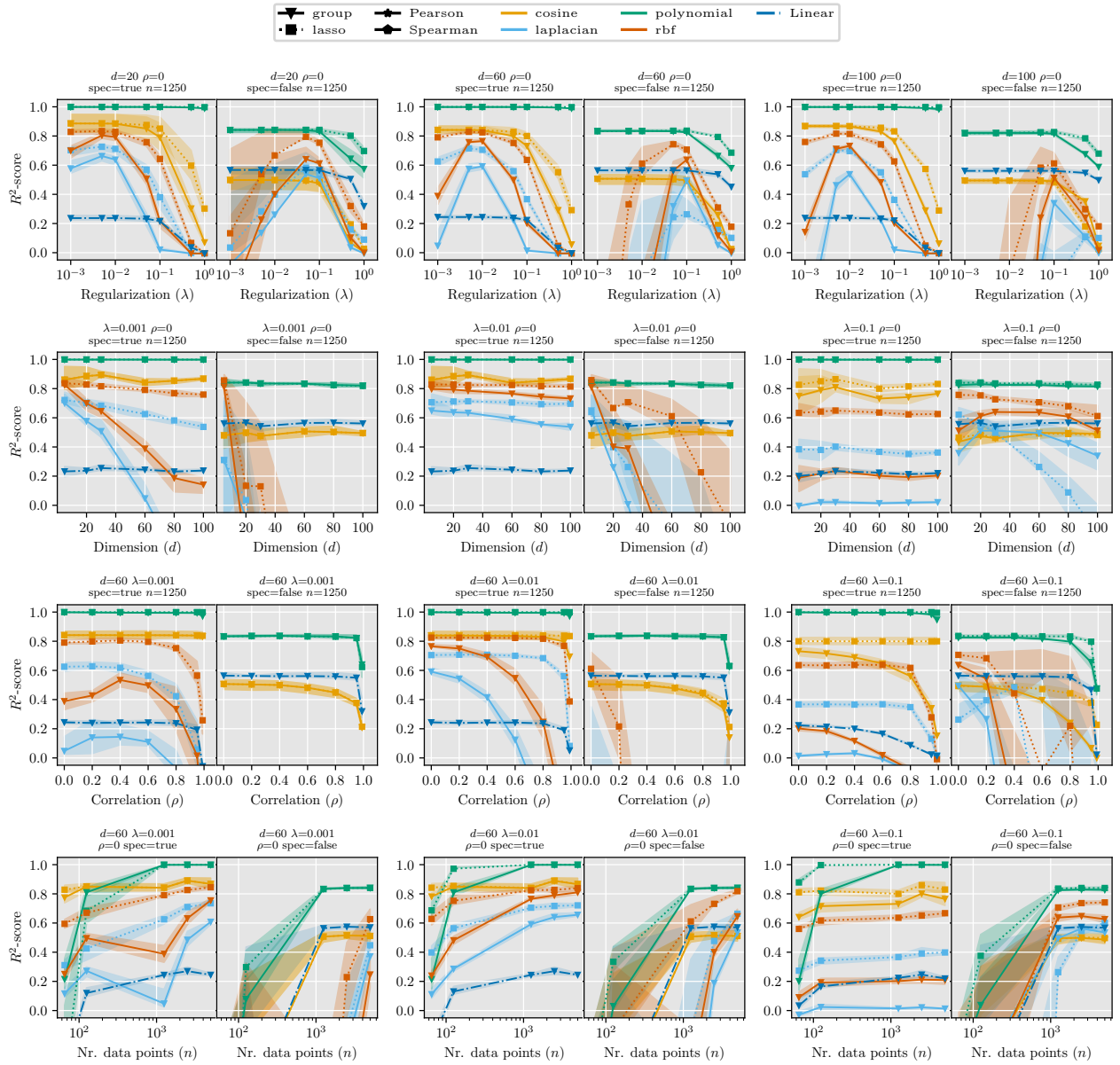


Figure 14: R^2 -score on the diagonal using Kernels

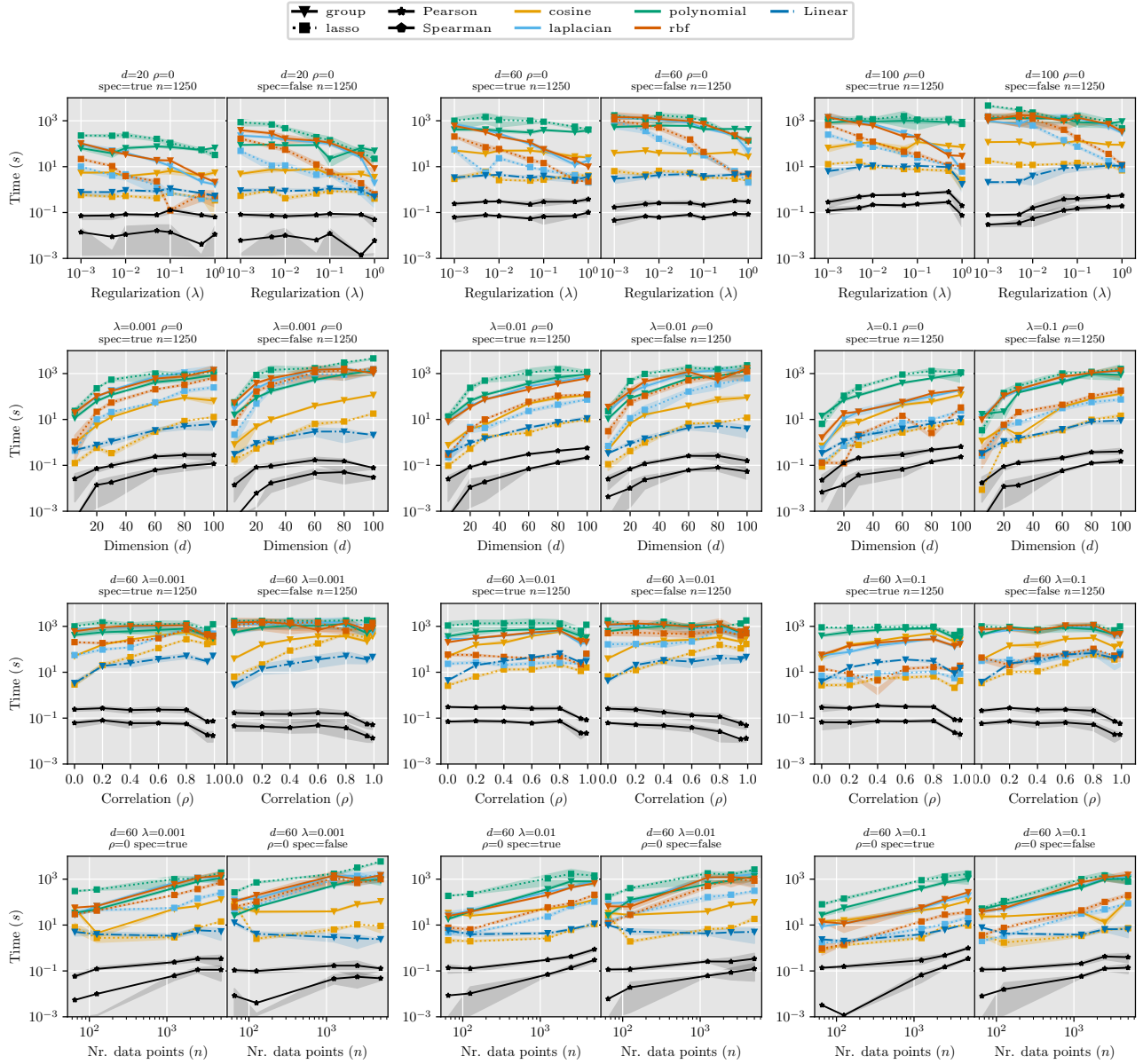


Figure 15: Execution times using kernels

Table 8: Permutation Errors for the encodings learned in the Action/Temporal sparsity datasets and the Temporal Causal3DIdent datasets. We report the mean and standard deviation over 50 random seeds and in each column we write the best method in **bold**.

Model	Method	Permutation Error \downarrow (n)					
		5	10	20	100	1000	10000
Action Sparsity Dataset							
DMS-VAE	NN	0.18 \pm 0.02	0.03 \pm 0.01	0.01 \pm 0.01	0.00 \pm 0.00	0.00 \pm 0.00	0.00 \pm 0.00
	Pearson	0.31 \pm 0.02	0.04 \pm 0.01	0.00 \pm 0.00	0.00 \pm 0.00	0.00 \pm 0.00	0.00 \pm 0.00
	Spearman	0.28 \pm 0.03	0.04 \pm 0.01	0.00 \pm 0.00	0.00 \pm 0.00	0.00 \pm 0.00	0.00 \pm 0.00
	Linear	0.25 \pm 0.03	0.03 \pm 0.01	0.00 \pm 0.00	0.00 \pm 0.00	0.00 \pm 0.00	0.00 \pm 0.00
	Spline	0.36 \pm 0.02	0.28 \pm 0.03	0.02 \pm 0.01	0.00 \pm 0.00	0.00 \pm 0.00	0.00 \pm 0.00
	RFF	0.47 \pm 0.02	0.11 \pm 0.02	0.02 \pm 0.01	0.00 \pm 0.00	0.00 \pm 0.00	0.00 \pm 0.00
	Laplacian	0.64 \pm 0.03	0.28 \pm 0.03	0.03 \pm 0.01	0.00 \pm 0.00	0.00 \pm 0.00	0.00 \pm 0.00
	Two Stage	0.46 \pm 0.03	0.06 \pm 0.02	0.02 \pm 0.01	0.00 \pm 0.00	0.00 \pm 0.00	0.00 \pm 0.00
iVAE	NN	0.82 \pm 0.02	0.72 \pm 0.02	0.53 \pm 0.02	0.38 \pm 0.02	0.24 \pm 0.01	0.20 \pm 0.00
	Pearson	0.76 \pm 0.02	0.56 \pm 0.02	0.39 \pm 0.02	0.35 \pm 0.02	0.16 \pm 0.02	0.14 \pm 0.01
	Spearman	0.75 \pm 0.02	0.64 \pm 0.02	0.50 \pm 0.02	0.31 \pm 0.03	0.18 \pm 0.03	0.10 \pm 0.02
	Linear	0.78 \pm 0.02	0.56 \pm 0.02	0.41 \pm 0.02	0.20 \pm 0.03	0.02 \pm 0.01	0.00 \pm 0.00
	Spline	0.84 \pm 0.02	0.77 \pm 0.02	0.61 \pm 0.02	0.32 \pm 0.02	0.12 \pm 0.02	0.00 \pm 0.00
	RFF	0.83 \pm 0.02	0.76 \pm 0.02	0.63 \pm 0.02	0.37 \pm 0.03	0.19 \pm 0.02	0.18 \pm 0.02
	Laplacian	0.84 \pm 0.02	0.78 \pm 0.02	0.65 \pm 0.02	0.34 \pm 0.02	0.03 \pm 0.01	0.00 \pm 0.00
	Two Stage	0.78 \pm 0.02	0.65 \pm 0.02	0.54 \pm 0.02	0.32 \pm 0.03	0.21 \pm 0.02	0.22 \pm 0.03
Temporal Sparsity Dataset							
DMS-VAE	NN	0.78 \pm 0.02	0.70 \pm 0.02	0.48 \pm 0.02	0.46 \pm 0.01	0.20 \pm 0.00	0.00 \pm 0.00
	Pearson	0.68 \pm 0.02	0.40 \pm 0.02	0.23 \pm 0.03	0.20 \pm 0.03	0.03 \pm 0.02	0.00 \pm 0.00
	Spearman	0.72 \pm 0.02	0.53 \pm 0.02	0.40 \pm 0.02	0.11 \pm 0.02	0.00 \pm 0.00	0.00 \pm 0.00
	Linear	0.67 \pm 0.02	0.41 \pm 0.03	0.20 \pm 0.03	0.07 \pm 0.02	0.00 \pm 0.00	0.00 \pm 0.00
	Spline	0.72 \pm 0.02	0.70 \pm 0.02	0.47 \pm 0.03	0.17 \pm 0.03	0.03 \pm 0.01	0.00 \pm 0.00
	RFF	0.76 \pm 0.02	0.59 \pm 0.02	0.37 \pm 0.03	0.10 \pm 0.02	0.03 \pm 0.02	0.01 \pm 0.01
	Laplacian	0.80 \pm 0.02	0.67 \pm 0.02	0.45 \pm 0.02	0.15 \pm 0.03	0.01 \pm 0.01	0.00 \pm 0.00
	Two Stage	0.78 \pm 0.02	0.59 \pm 0.03	0.44 \pm 0.02	0.15 \pm 0.02	0.01 \pm 0.01	0.00 \pm 0.00
TCVAE	NN	0.83 \pm 0.02	0.81 \pm 0.02	0.65 \pm 0.02	0.33 \pm 0.01	0.25 \pm 0.02	0.60 \pm 0.00
	Pearson	0.74 \pm 0.02	0.54 \pm 0.03	0.30 \pm 0.03	0.36 \pm 0.03	0.24 \pm 0.03	0.23 \pm 0.02
	Spearman	0.77 \pm 0.02	0.61 \pm 0.03	0.47 \pm 0.03	0.28 \pm 0.03	0.14 \pm 0.03	0.01 \pm 0.01
	Linear	0.76 \pm 0.02	0.50 \pm 0.02	0.36 \pm 0.03	0.26 \pm 0.03	0.18 \pm 0.02	0.19 \pm 0.03
	Spline	0.79 \pm 0.02	0.72 \pm 0.02	0.48 \pm 0.02	0.32 \pm 0.03	0.24 \pm 0.03	0.15 \pm 0.02
	RFF	0.81 \pm 0.02	0.60 \pm 0.02	0.44 \pm 0.03	0.30 \pm 0.03	0.29 \pm 0.03	0.23 \pm 0.03
	Laplacian	0.83 \pm 0.02	0.70 \pm 0.02	0.53 \pm 0.03	0.32 \pm 0.03	0.22 \pm 0.03	0.12 \pm 0.03
	Two Stage	0.80 \pm 0.02	0.64 \pm 0.02	0.52 \pm 0.02	0.32 \pm 0.03	0.22 \pm 0.03	0.08 \pm 0.03
Temporal Causal3DIdent Dataset							
CITRIS-VAE	NN	0.72 \pm 0.02	0.37 \pm 0.03	0.11 \pm 0.02	0.00 \pm 0.00	0.00 \pm 0.00	0.00 \pm 0.00
	Pearson	0.77 \pm 0.02	0.61 \pm 0.03	0.42 \pm 0.02	0.34 \pm 0.02	0.14 \pm 0.02	0.00 \pm 0.00
	Spearman	0.70 \pm 0.02	0.55 \pm 0.03	0.44 \pm 0.02	0.16 \pm 0.02	0.10 \pm 0.02	0.01 \pm 0.00
	Linear	0.71 \pm 0.02	0.49 \pm 0.02	0.34 \pm 0.02	0.03 \pm 0.01	0.00 \pm 0.00	0.00 \pm 0.00
	Spline	0.74 \pm 0.02	0.64 \pm 0.02	0.35 \pm 0.02	0.01 \pm 0.00	0.00 \pm 0.00	0.00 \pm 0.00
	RFF	0.81 \pm 0.02	0.70 \pm 0.02	0.48 \pm 0.02	0.18 \pm 0.02	0.10 \pm 0.02	0.06 \pm 0.02
	Laplacian	0.77 \pm 0.02	0.61 \pm 0.02	0.44 \pm 0.01	0.15 \pm 0.02	0.00 \pm 0.00	0.00 \pm 0.00
	Two Stage	0.76 \pm 0.02	0.65 \pm 0.02	0.47 \pm 0.03	0.17 \pm 0.02	0.07 \pm 0.02	0.01 \pm 0.00
iVAE	NN	0.73 \pm 0.03	0.46 \pm 0.03	0.29 \pm 0.02	0.00 \pm 0.00	0.00 \pm 0.00	0.00 \pm 0.00
	Pearson	0.63 \pm 0.04	0.47 \pm 0.03	0.26 \pm 0.03	0.24 \pm 0.03	0.00 \pm 0.00	0.00 \pm 0.00
	Spearman	0.71 \pm 0.03	0.50 \pm 0.03	0.39 \pm 0.02	0.11 \pm 0.02	0.00 \pm 0.00	0.00 \pm 0.00
	Linear	0.70 \pm 0.03	0.45 \pm 0.03	0.24 \pm 0.03	0.00 \pm 0.00	0.00 \pm 0.00	0.00 \pm 0.00
	Spline	0.69 \pm 0.03	0.62 \pm 0.03	0.41 \pm 0.03	0.02 \pm 0.01	0.00 \pm 0.00	0.00 \pm 0.00
	RFF	0.73 \pm 0.03	0.54 \pm 0.03	0.39 \pm 0.03	0.02 \pm 0.01	0.00 \pm 0.00	0.00 \pm 0.00
	Laplacian	0.69 \pm 0.03	0.49 \pm 0.03	0.32 \pm 0.03	0.01 \pm 0.01	0.00 \pm 0.00	0.00 \pm 0.00
	Two Stage	0.75 \pm 0.03	0.55 \pm 0.03	0.36 \pm 0.02	0.08 \pm 0.02	0.00 \pm 0.00	0.00 \pm 0.00

Table 9: R^2 scores for the encodings learned in the Action/Temporal sparsity datasets and the Temporal Causal3DIdent datasets. We report the mean and standard deviation over 50 random seeds and in each column we write the best method in **bold**. If a score was below -100 , we indicate this with †.

Model	Method	R^2 -score on the diagonal \uparrow (n)					
		5	10	20	100	1000	10000
Action Sparsity Dataset							
DMS-VAE	NN	0.21 \pm 0.03	0.56 \pm 0.01	0.68 \pm 0.00	0.78 \pm 0.00	0.79 \pm 0.00	0.79 \pm 0.00
	Pearson	-	-	-	-	-	-
	Spearman	-	-	-	-	-	-
	Linear	-0.29 \pm 0.13	0.56 \pm 0.02	0.72 \pm 0.00	0.77 \pm 0.00	0.77 \pm 0.00	0.77 \pm 0.00
	Spline	†	0.08 \pm 0.02	0.53 \pm 0.01	0.78 \pm 0.00	0.78 \pm 0.00	0.79 \pm 0.00
	RFF	-0.69 \pm 0.12	0.24 \pm 0.02	0.59 \pm 0.01	0.77 \pm 0.00	0.78 \pm 0.00	0.78 \pm 0.00
	Laplacian	-0.72 \pm 0.08	-0.03 \pm 0.02	0.33 \pm 0.01	0.64 \pm 0.01	0.70 \pm 0.00	0.70 \pm 0.00
	Two Stage	†	-1.25 \pm 1.41	0.53 \pm 0.08	0.77 \pm 0.00	0.79 \pm 0.00	0.79 \pm 0.00
iVAE	NN	-0.36 \pm 0.03	-0.14 \pm 0.03	0.10 \pm 0.01	0.29 \pm 0.00	0.31 \pm 0.00	0.31 \pm 0.00
	Pearson	-	-	-	-	-	-
	Spearman	-	-	-	-	-	-
	Linear	-0.86 \pm 0.11	-0.10 \pm 0.02	0.14 \pm 0.01	0.25 \pm 0.00	0.27 \pm 0.00	0.28 \pm 0.00
	Spline	-19.24 \pm 13.32	-0.18 \pm 0.02	0.05 \pm 0.01	0.24 \pm 0.00	0.27 \pm 0.00	0.27 \pm 0.00
	RFF	-0.93 \pm 0.10	-0.22 \pm 0.02	-0.02 \pm 0.01	0.19 \pm 0.00	0.25 \pm 0.00	0.25 \pm 0.00
	Laplacian	-0.83 \pm 0.06	-0.23 \pm 0.02	-0.05 \pm 0.01	0.12 \pm 0.00	0.17 \pm 0.00	0.17 \pm 0.00
	Two Stage	†	-1.49 \pm 0.19	-0.28 \pm 0.03	0.19 \pm 0.01	0.30 \pm 0.00	0.31 \pm 0.00
Temporal Sparsity Dataset							
DMS-VAE	NN	-2.78 \pm 0.30	-0.26 \pm 0.03	0.17 \pm 0.01	0.38 \pm 0.00	0.42 \pm 0.00	0.43 \pm 0.00
	Pearson	-	-	-	-	-	-
	Spearman	-	-	-	-	-	-
	Linear	-0.94 \pm 0.11	0.11 \pm 0.02	0.32 \pm 0.01	0.41 \pm 0.00	0.43 \pm 0.00	0.43 \pm 0.00
	Spline	-6.88 \pm 4.87	-0.16 \pm 0.03	0.17 \pm 0.01	0.40 \pm 0.00	0.42 \pm 0.00	0.43 \pm 0.00
	RFF	-1.00 \pm 0.11	-0.10 \pm 0.03	0.21 \pm 0.01	0.39 \pm 0.00	0.41 \pm 0.00	0.42 \pm 0.00
	Laplacian	-1.11 \pm 0.12	-0.22 \pm 0.03	0.04 \pm 0.01	0.24 \pm 0.01	0.30 \pm 0.00	0.31 \pm 0.00
	Two Stage	†	-1.24 \pm 0.19	-0.11 \pm 0.05	0.32 \pm 0.01	0.43 \pm 0.00	0.43 \pm 0.00
TCVAE	NN	-3.02 \pm 0.24	-0.44 \pm 0.04	0.05 \pm 0.01	0.28 \pm 0.00	0.33 \pm 0.00	0.34 \pm 0.00
	Pearson	-	-	-	-	-	-
	Spearman	-	-	-	-	-	-
	Linear	-1.00 \pm 0.15	0.00 \pm 0.03	0.23 \pm 0.01	0.32 \pm 0.00	0.33 \pm 0.00	0.33 \pm 0.00
	Spline	†	-0.18 \pm 0.02	0.10 \pm 0.01	0.30 \pm 0.00	0.33 \pm 0.00	0.34 \pm 0.00
	RFF	-0.84 \pm 0.08	-0.13 \pm 0.03	0.15 \pm 0.01	0.31 \pm 0.00	0.33 \pm 0.00	0.33 \pm 0.00
	Laplacian	-0.92 \pm 0.10	-0.21 \pm 0.03	-0.01 \pm 0.01	0.17 \pm 0.01	0.23 \pm 0.00	0.23 \pm 0.00
	Two Stage	†	-1.54 \pm 0.21	-0.25 \pm 0.07	0.21 \pm 0.01	0.33 \pm 0.00	0.34 \pm 0.00
Temporal Causal3DIdent Dataset							
CITRIS-VAE	NN	-4.11 \pm 0.32	-0.17 \pm 0.04	0.22 \pm 0.02	0.42 \pm 0.01	0.59 \pm 0.00	0.65 \pm 0.00
	Pearson	-	-	-	-	-	-
	Spearman	-	-	-	-	-	-
	Linear	-1.44 \pm 0.30	-0.35 \pm 0.14	0.16 \pm 0.01	0.38 \pm 0.00	0.43 \pm 0.00	0.44 \pm 0.00
	Spline	†	-0.33 \pm 0.08	0.09 \pm 0.01	0.40 \pm 0.00	0.52 \pm 0.00	0.55 \pm 0.00
	RFF	-1.42 \pm 0.29	-0.39 \pm 0.09	-0.04 \pm 0.01	0.23 \pm 0.01	0.41 \pm 0.01	0.45 \pm 0.00
	Laplacian	-1.37 \pm 0.30	-0.37 \pm 0.09	-0.04 \pm 0.01	0.31 \pm 0.00	0.47 \pm 0.00	0.49 \pm 0.00
	Two Stage	†	-7.78 \pm 2.92	-0.84 \pm 0.09	-0.56 \pm 0.04	0.48 \pm 0.00	0.54 \pm 0.00
iVAE	NN	-4.29 \pm 0.36	-0.23 \pm 0.05	0.13 \pm 0.02	0.62 \pm 0.00	0.71 \pm 0.00	0.74 \pm 0.00
	Pearson	-	-	-	-	-	-
	Spearman	-	-	-	-	-	-
	Linear	-0.88 \pm 0.16	-0.20 \pm 0.03	0.14 \pm 0.01	0.43 \pm 0.00	0.47 \pm 0.00	0.48 \pm 0.00
	Spline	†	-0.41 \pm 0.15	0.01 \pm 0.01	0.43 \pm 0.00	0.55 \pm 0.00	0.56 \pm 0.00
	RFF	-0.84 \pm 0.14	-0.26 \pm 0.03	-0.01 \pm 0.01	0.36 \pm 0.01	0.52 \pm 0.00	0.54 \pm 0.00
	Laplacian	-0.81 \pm 0.14	-0.24 \pm 0.03	0.00 \pm 0.01	0.34 \pm 0.01	0.49 \pm 0.00	0.51 \pm 0.00
	Two Stage	†	†	-0.74 \pm 0.11	-0.50 \pm 0.06	0.54 \pm 0.00	0.56 \pm 0.00

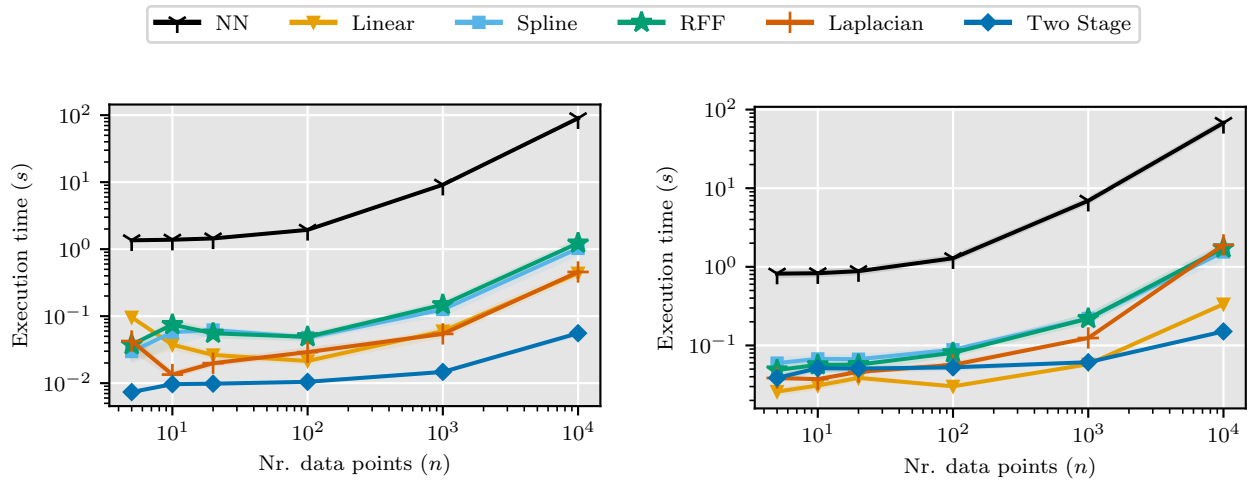


Figure 16: Execution times of the baseline and multiple versions of our estimator on the causal variables and encodings learned based on the Action/Temporal Sparsity Dataset and the Temporal Causal3DIdent dataset